JOURNAL OF PETROLOGY | VOLUME 46 | NUMBER 1 | PAGES 135–167 | 2005 | doi:10.1093/petrology/egh066

An Experimental Investigation of the Influence of Water and Oxygen Fugacity on Differentiation of MORB at 200 MPa

JASPER BERNDT*, JÜRGEN KOEPKE AND FRANÇOIS HOLTZ

INSTITUT FÜR MINERALOGIE, UNIVERSITÄT HANNOVER, WELFENGARTEN 1, D-30167 HANNOVER, GERMANY

RECEIVED APRIL 15, 2002; ACCEPTED JULY 28, 2004
ADVANCE ACCESS PUBLICATION OCTOBER 1, 2004

Crystallization experiments were performed at 200 MPa in the temperature range 1150–950°C at oxygen fugacities corresponding to the quartz–fayalite–magnetite (QFM) and $MnO–Mn_3O_4$ buffers to assess the role of water and f_{O_2} on phase relations and differentiation trends in mid-ocean ridge basalt (MORB) systems. Starting from a primitive (MgO 9·8 wt %) and an evolved MORB (MgO 6·49 wt %), crystallization paths with four different water contents (0·35–4·7 wt % H_2O) have been investigated. In primitive MORB, olivine is the liquidus phase followed by plagioclase + clinopyroxene. Amphibole is present only at water-saturated conditions below 1000°C, but not all fluid-saturated runs contain amphibole. Magnetite and orthopyroxene are not stable at low f_{O_2} (QFM buffer). Residual liquids obtained at low f_{O_2} show a tholeiitic differentiation trend. The crystallization of magnetite at high f_{O_2} ($MnO–Mn_3O_4$ buffer) results in a decrease of melt FeO/MgO ratio, causing a calc-alkaline differentiation trend. Because the magnetite crystallization temperature is nearly independent of the H_2O content, in contrast to silicate minerals, the calc-alkaline differentiation trend is more pronounced at high water contents. Residual melts at 950°C in a primitive MORB system have compositions approaching those of oceanic plagiogranites in terms of SiO_2 and K_2O, but have Ca/Na ratios and FeO* contents that are too high compared with the natural rocks, implying that fractionation processes are necessary to reach typical compositions of natural oceanic plagiogranites.*

KEY WORDS: *differentiation; MORB; oxygen fugacity; water activity; oceanic plagiogranite*

INTRODUCTION

Since the late 1950s, many experimental studies have focused on the investigation of phase relations in natural basaltic systems for a better understanding of the differentiation mechanisms under crustal pressures and temperatures. Most of these experiments have been carried out at 1 atm (e.g. Osborn, 1959; Grove & Bryan, 1983; Grove & Baker, 1984; Juster *et al.*, 1989; Snyder *et al.*, 1993; Thy & Lofgren, 1994; Toplis & Carroll, 1995, 1996), assuming that the small pressure difference between shallow magma chambers and the surface does not influence significantly the results and implications drawn from these studies. It was considered that the low volatile content of basaltic melts (volatiles are incorporated in melts only under pressure) has little influence on phase relations. One of the benefits of these studies was to evaluate the role of f_{O_2} (oxygen fugacity), which is a critical parameter controlling the crystallization of Fe–Ti oxides in iron-bearing systems.

Concerning the role of volatiles, especially H_2O, the broad absence of amphibole as a primary cumulate phase in tholeiitic plutonic complexes (e.g. Skaergaard, Kiglapait, Pleasant Bay, typical oceanic crust) has been taken as evidence for very low water activities during the main stage of fractionation of these melts. However, the common presence of small amounts of interstitial amphibole within typical oceanic gabbros indicates that water may play a role, at least during the late differentiation stage of mid-ocean ridge basalt (MORB) (e.g. Gillis, 1996; Dick *et al.*, 2000; Coogan *et al.*, 2001). Studies on water contents in basalts by Sobolev & Chaussidon (1996), Danyushevsky *et al.* (2000) and Kovalenko *et al.* (2000) showed that even for primitive MORB the H_2O content varies from <0·1 up to 1·5 wt %. Assuming an initial water content for a primitive MORB liquid of 0·5 wt % at a pressure corresponding to shallow levels, the crystallization of 60 wt % of anhydrous minerals

*Corresponding author. Present address: Institut für Mineralogie, Westfälische Wilhelms-Universität Münster, Corrensstrasse 24, D-48149 Münster, Germany. Telephone: +49 (0)251 83 33049. Fax: +49 (0)251 83 38397. E-mail: jberndt@uni-muenster.de

Table 1: Composition of natural primitive MORB and synthetic MORB B1 and B2 (starting material)

	n[a]	SiO_2	TiO_2	Al_2O_3	FeO*[b]	MnO	MgO	CaO	Na_2O	K_2O	P_2O_5
Natural MORB[c]		49·47[b] (16)[d]	0·83 (10)	16·35 (54)	8·71 (49)	0·16 (9)	9·80 (26)	12·35 (33)	2·16 (12)	0·07 (5)	0·09 (5)
Synthetic MORB B1	18	49·64 (27)	0·87 (5)	16·07 (16)	8·63 (7)	0·15 (7)	9·77 (9)	12·44 (16)	2·28 (9)	0·08 (3)	0·08 (5)
Glass of run 42	10	51·38 (57)	1·46 (11)	15·97 (57)	10·98 (25)	0·19 (15)	6·16 (29)	10·50 (30)	3·06 (24)	0·12 (7)	0·18 (12)
Synthetic MORB B2	12	51·17 (23)	1·43 (6)	15·93 (16)	10·72 (26)	0·21 (7)	6·49 (7)	10·57 (13)	3·13 (11)	0·15 (4)	0·19 (7)

[a]Number of analyses.
[b]Oxide concentrations from microprobe are normalized to 100 wt % with all Fe as FeO* (total iron).
[c]Average composition of primitive MORB compositions from: Frey *et al*. (1974), Bryan & Moore (1977) and Natland & Melson (1980), all cited by Elthon (1991); Langmuir *et al*. (1977); Spulber & Rutherford (1983) and Christie & Sinton (1986), cited by Brooks *et al*. (1991); McKenzie & Bickle (1988).
[d]Numbers in parentheses are one standard deviation of replicate analyses in terms of least units cited.

results in an increase of water activity (a_{H_2O}) up to about 0·23 [calculated after Burnham (1979) for MORB at 1100°C and 100 MPa; see below]. Thus, it can be expected that the water activity of MORB liquids increases with differentiation to values that influence phase relations in these systems (especially at high degrees of fractionation), even if the stability field of amphibole may not have been reached.

Few experimental data are available to understand the effect of a_{H_2O} on the differentiation trends of primitive MORBs at moderate pressure (e.g. $\leq$200 MPa). Spulber & Rutherford (1983) performed experiments using a primitive MORB from the Galapagos Spreading Centre to assess the origin of plagiogranites in oceanic ridges, but a_{H_2O} was not varied systematically. Further experimental investigations have been carried out in more alkali-rich compositions. The comparison of results from melting and crystallization experiments of Holloway & Burnham (1972) on the 1921 Kilauea tholeiite at $a_{H_2O} \sim 0{\cdot}6$ with those of Yoder & Tilley (1962) and Helz (1973, 1976), at water-saturated conditions, shows that water influences phase relations and that the occurrence of amphibole influences the differentiation from andesitic to rhyolitic residual melts. Sisson & Grove (1993*a*, 1993*b*) investigated phase relations in calc-alkaline systems at water-saturated conditions, and Kawamoto (1996) carried out melting experiments at $a_{H_2O} \leq 1$ in similar systems. Those workers emphasized the dramatic role of water and pointed out that the absence of amphibole in these systems does not necessarily mean that dry conditions are prevailing.

The lack of experiments in basaltic systems at moderate pressure (100–500 MPa) in the presence of volatiles is due to experimental problems. The formation of quench crystals is a serious problem when performing experiments with low-viscosity basaltic compositions, and often hampers the interpretation of results from phase equilibrium studies (e.g. Hamilton *et al*., 1964; Holloway & Burnham, 1972; Helz, 1973, 1976). In this study, all experiments were carried out in internally heated pressure vessels (IHPV) using a rapid-quench sample holder to avoid the formation of quench crystals during cooling of the experimental charge (Holloway *et al*., 1992; Roux & Lefevre, 1992; Berndt *et al*., 2002). A first series of experiments was undertaken to provide information on the influence of a_{H_2O} on phase relations in a primitive MORB system at 200 MPa and f_{O_2} corresponding to the MnO–Mn_3O_4 buffer using both a primitive and a fractionated synthetic 10-component MORB glass (Table 1). As the f_{O_2} of natural MORB lavas is found to vary generally between QFM − 2 and QFM + 1 (where QFM is the quartz–fayalite–magnetite buffer) (e.g. Carmichael & Ghiorso, 1986; Christie *et al*., 1986), we performed a second series of crystallization experiments under redox conditions corresponding to the QFM buffer. For these experiments, the sample holder was equipped with a hydrogen membrane to control and adjust f_{O_2} (Berndt *et al*., 2002). All experiments were performed in the temperature range 1150–950°C and at 200 MPa, a typical pressure of MORB magma chambers under the mid-ocean ridge system at depths between 3 and 6 km (e.g. Fisk, 1984; Nicolas, 1989). For a better understanding of the role of water during differentiation of MORB, the initial water content of our experimental systems was varied systematically ranging from 0·35 wt % to 4·7 wt % H_2O. The results are used to estimate the influence of H_2O and f_{O_2} on stability of Fe–Ti oxides and MORB liquid line of descent.

EXPERIMENTAL TECHNIQUES

Apparatus

All experiments were performed in a large-volume IHPV working vertically with pure Ar or Ar–H_2 mixtures as pressure medium. A detailed description of the apparatus

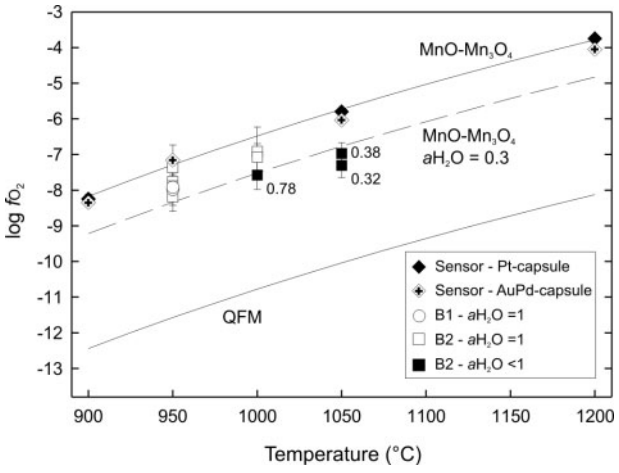

Fig. 1. Intrinsic f_{O_2} of the IHPV measured by solid sensor technique after Taylor *et al.* (1992) and calculated f_{O_2} using coexisting magnetite–ilmenite pairs (Andersen *et al.*, 1993) from runs at intrinsic conditions. Continuous lines show MnO–Mn_3O_4 and QFM buffer curve. Dashed line shows the shift of f_{O_2} relative to the MnO–Mn_3O_4 buffer curve at lower water activities ($a_{H_2O} = 0{\cdot}3$) and more reducing conditions in the experiments. NiPd sensor measurements after Taylor *et al.* (1992) were performed using both Pt and $Au_{80}Pd_{20}$ capsules.

has been given by Berndt *et al.* (2002). Formation of quench crystals during cooling the experimental charge was avoided using a rapid-quench system [see experimental setup described by Berndt *et al.* (2002)] in which up to six capsules are fixed to a Pt-wire in the hot zone of the furnace. By fusing the Pt-wire, the capsules drop onto a cold copper block placed at the bottom of the sample holder (about 25°C). The intrinsic f_{O_2} (pure Ar as pressure medium) of the IHPV has been measured at four temperatures (900–1200°C) using the Ni–Pd solid redox sensor technique after Taylor *et al.* (1992) and is equivalent to the MnO–Mn_3O_4 solid oxygen buffer (Fig. 1).

Starting material

For experiments under oxidizing conditions (MnO–Mn_3O_4 buffer) two synthetic starting compositions (Table 1) were used for the crystallization experiments: a primitive MORB glass (B1) and a more evolved MORB glass (B2) corresponding to a residual glass composition obtained after 50% crystallization of B1 at 1100°C (run 42; Table 1). Only the B1 composition was used for experiments under reducing conditions (QFM buffer). Starting materials were made from synthetic oxide and carbonate powders. Oxide powder mixtures were placed into a Pt crucible and fused twice (grinding between fusions) at 1600°C, 1 atm, and a log f_{O_2} corresponding to about −0·68 (air). To avoid alkali loss from the glass, melting duration was <1·5 h. Electron microprobe analyses of chips extracted from the top, middle and bottom of the glass showed that they are homogeneous. The glass B1 lies within the compositional range of natural primitive MORBs (Table 1).

Sample preparation and experimental procedure

First attempts were made by preparing the samples with dry powder of the starting glasses (grain size <50 μm) and a given amount of water added into $Au_{80}Pd_{20}$ capsules. After loading the capsules into the sample holder, they were held for about 1 h above the liquidus temperature at 200 MPa to obtain a homogeneous distribution of H_2O in the melt and to allow redox equilibrium of the melt. In a second step, temperature was lowered to the desired run temperature. Resulting products clearly showed disequilibrium features such as complex zonation of minerals. Compositional variations for Al_2O_3 in clinopyroxene were as high as 5–9 wt % within a single crystal. To avoid these effects, charges with dry glass plus water were brought directly to the desired run temperature. Results at relatively high temperatures (1050–1150°C) did not show disequilibrium features, but mineral sizes and distributions were heterogeneous at lower temperatures and low water activity (a_{H_2O}). This is probably due to crystallization taking place before homogeneous distribution of water is achieved in the glass powder.

Therefore, the experimental strategy consisted in using pre-hydrated glass powder as starting materials (Gaetani & Grove, 1998; Müntener *et al.*, 2001). Large amounts of dry glass powder were placed into $Au_{80}Pd_{20}$ capsules [internal diameter (i.d.) 0·5 cm; outer diameter (o.d.) 0·54 cm at 3 cm length] and stuffed with the help of a steel piston. Distilled water was added to the charge using a microsyringe in five steps to achieve homogeneous H_2O distribution within the capsule. Sealed capsules were heated at 1250°C and 200 MPa (above the liquidus) at the desired f_{O_2} (either MnO–Mn_3O_4 or QFM buffer conditions) for 24 h in an IHPV equipped with the rapid-quench hydrogen-membrane device described above. Homogeneous crystal- and bubble-free glasses were obtained and the water contents were determined by Karl–Fischer titration (KFT) (Table 2; for technique and precision see Behrens (1995)]. Final bulk water contents of the glasses vary between 0·35 and 4·7 wt % and are shown in Table 3.

The pre-hydrated glasses were finally crushed in a steel mortar and sieved to fractions of 100–200 μm. About 50–80 mg of the hydrous glass powders were sealed in $Au_{80}Pd_{20}$ capsules (i.d. 0·3 cm; o.d. 0·34 cm at 1 cm length). A set of up to four capsules (corresponding to the four bulk H_2O contents of B1 and B2) were fixed to the rapid-quench device and brought directly to run temperature. Phase relations were investigated at 200 MPa, at 50°C intervals in the temperature range 1150–950°C (Table 3). The run durations for oxidizing experiments were ~20 h, except for charges 62 and 61 (B1; 72 h) and 111 (B2; 96 h). The products of these longer experiments were compared with those of the 20 h runs conducted at the same pressure and temperature

Table 2: Comparison between water solubility measured by Karl–Fischer titration (KFT) analysis and calculated by the thermodynamic model of Burnham (1979) assuming $a_{H_2O} = 1$ *for MORB at 200 MPa*

	wt % H_2O	
	KFT analysis	Burnham model
$MnO-Mn_3O_4$ buffer; 200 MPa; 1250°C		
B1[a]	4·70 ± 0·09	4·54
B2	4·50 ± 0·10	4·57
QFM buffer; 203 MPa; 1200°C[b]		
B1	4·46 ± 0·02	4·50

[a]B1 and B2 represent starting compositions used in this study (Table 1).
[b]Data from Berndt *et al.* (2002).

confirming identical results (runs 45, 42 and 104; see below and Table 3a and b). Experimental duration for runs under reducing conditions was limited by the diffusive Fe loss to the capsule material and varied with temperature from 2 to 9·2 h (Table 3c). After quenching each capsule was weighed to check for leaks and then punctured to determine if a fluid phase was present or not. A cross-section of each capsule (including the sample container) was prepared as a polished section for electron microprobe analysis of solid phases and the noble metal.

Loss of iron

To avoid iron loss to the sample container (e.g. Johannes & Bode, 1978; Sisson & Grove, 1993*a*), $Au_{80}Pd_{20}$ capsules were used because Fe solubility is lower in $Au_{80}Pd_{20}$ than in Pt, and $Au_{80}Pd_{20}$ has a higher melting point than pure Au, which allowed us to perform experiments up to 1250°C (Kawamoto & Hirose, 1994). The glasses and capsule walls were analysed with the electron microprobe to check for iron loss or enrichment, respectively. No iron was detected in the capsule material of experiments performed under oxidizing conditions and the total Fe content of the hydrous glasses was equivalent to that of the dry starting material. Experiments performed under QFM buffer conditions showed significant iron loss as a result of Fe diffusion into the $Au_{80}Pd_{20}$ capsule material. Therefore, the $Au_{80}Pd_{20}$ capsules were pre-saturated in iron at f_{O_2} corresponding to the QFM buffer at 200 MPa and 1200°C (conditions similar to the desired f_{O_2} in the crystallization experiments at $a_{H_2O} = 1$) following the procedure described by Ford (1978). Thus, iron loss could be limited in our study. A melt composition profile of run 130 (Table 3c), performed above the liquidus temperature at 1150°C and with about 4·58 wt % H_2O melt water content, showed that iron has been lost mainly from the rim of the experimental charge, which is in direct contact with the capsule material. In the middle of the capsule the initial iron concentration of the glass was preserved. The average iron content along the profile was lowered by about 4·8% relative to the starting material. Iron loss from the other experiments performed at 1150°C was estimated to be between 6 and 8% relative by mass balance calculations. At temperatures below 1100°C, Spulber & Rutherford (1983) and Sisson & Grove (1993*a*) emphasized that no significant amount of iron was lost from their samples to the capsule material, which is in accordance with our results. Therefore, the iron content of the glasses analysed in the middle of the capsule is believed to be realistic. This is confirmed by Fe^{2+}–Mg olivine–melt partition coefficients, which agree with published data for this mineral.

Calculations of a_{H_2O} and f_{O_2}

It has been shown that the thermodynamic model of Burnham (1979) is not always correct for the calculation of a_{H_2O} and melt water contents, especially at high pressures (e.g. water solubility can be underestimated by 20% relative at 500 MPa; Holtz *et al.*, 1995). At 200 MPa, calculated H_2O solubilities after Burnham (1979) for synthesized MORB glasses B1 and B2 agree well with the contents determined by KFT for these glasses (Table 2). Thus, we have used the model of Burnham (1979) to calculate melt water content at $a_{H_2O} = 1$. In addition, for runs in which a_{H_2O} was <1, water activities have also been calculated using the model of Burnham (1979) and the water contents of the melts determined by mass balance and electron microprobe (see below).

For runs performed under oxidizing conditions the f_{H_2} was imposed by the vessel and corresponds to the MnO–Mn_3O_4 solid oxygen buffer [based on the equation of Chou (1978)]. For experiments at lower oxygen fugacities a proportion of H_2 was added to the pressure medium (Ar) to reach a final pH_2 at run conditions resulting in an f_{O_2} corresponding to the QFM buffer at water-saturated conditions (Table 3c). It should be noted that in water-undersaturated experiments f_{H_2O} and thus f_{O_2} decrease with a_{H_2O} (Scaillet *et al.*, 1995), resulting in much more reducing f_{O_2} conditions at low a_{H_2O} (Table 3).

Melt Fe^{2+}/Fe^{3+} ratios were calculated using the method of Kress & Carmichael (1991). As emphasized by Baker & Rutherford (1996) and Gaillard *et al.* (2001), the expression of Kress & Carmichael (1991) has not been calibrated for hydrous glasses. For H_2O-saturated rhyolitic melts Baker & Rutherford (1996) and Gaillard *et al.* (2001) showed that water has an oxidizing effect on the melt Fe^{2+}/Fe^{3+} ratio relative to the Kress & Carmichael (1991) expression, especially at $f_{O_2} < NNO + 1·5$ (where NNO is the nickel–nickel oxide buffer). For the hydrous experiments performed in this study at the QFM buffer (which is below the NNO buffer conditions), the

Table 3a: Experimental conditions and results for composition B1 (MnO–Mn_3O_4 buffer)

Run	wt % H_2O[a] bulk	wt % H_2O[b] in melt	a_{H_2O}	f_{H_2O} (bar)	log f_{O_2}[c] (bar)	ΔQFM[d] (bar)	Phases and modal proportions[e,f]							ΣR^2
1150° C; 205 MPa; 23·8 h														
66	4·70	4·55[g]	1	2074	−4·38	+4·33	gl(100)	fl						
65	2·53	2·56	0·47	971	−5·04	+3·67	gl(98·7)	ol(1·3)						0·52
64	1·49	1·54	0·21	441	−5·73	+2·99	gl(96·5)	ol(3·5)						0·30
63	0·89	1·01	0·10	214	−6·36	+2·36	gl(88·5)	ol(4·7)	cpx(2·6)	pl(4·2)				0·31
1100° C; 202 MPa; 21 h														
45	4·70	4·57[g]	1	2011	−5·03	+4·32	gl(98·2)	ol(1·8)	fl					0·42
44	2·53	3·13	0·61	1218	−5·47	+3·89	gl(80·8)	ol(5·2)	cpx(9·6)	pl(4·4)				0·52
43	1·49	2·45	0·43	861	−5·77	+3·59	gl(60·9)	ol(8·2)	cpx(15·4)	pl(15·5)				0·27
42	0·89	1·79	0·27	544	−6·17	+3·19	gl(49·6)	ol(8·9)	cpx(17·6)	pl(23·9)				0·15
1100° C; 204 MPa; 72 h														
62	4·70	4·56[g]	1	2029	−5·03	+4·32	gl(98·5)	ol(1·5)	fl					0·40
61	0·89	1·72	0·25	506	−6·24	+3·11	gl(51·8)	ol(8·6)	cpx(17·4)	pl(22·2)				0·21
1050° C; 202 MPa; 20·75 h														
41	4·70	4·73[g]	1	1964	−5·73	+4·31	gl(77·5)	ol(7·4)	cpx(10·5)	pl(3·9)	mt(0·7)	fl		0·33
40	2·53	4·84[g]	1	1964	−5·73	+4·31	gl(51·4)	ol(9·7)	cpx(18·1)	pl(18·8)	mt(2·0)	fl		0·35
39	1·49	3·63	0·70	1373	−6·04	+4·00	gl(41·0)	ol(8·9)	cpx(23·8)	pl(24·7)	mt(1·6)			0·20
38	0·89	2·34	0·38	752	−6·56	+3·48	gl(38·1)	ol(8·3)	cpx(24·7)	pl(26·4)	mt(2·5)			0·28
1000° C; 205 MPa; 20 h														
37	4·70	5·09[g]	1	1947	−6·48	+4·30	gl(47·6)	ol(5·8)	cpx(25·9)	pl(15·1)	mt(3·5)	am(2·1)	fl	0·17
36	2·53	5·08[g]	1	1947	−6·48	+4·30	gl(34·7)	ol(8·0)	cpx(25·8)	pl(27·7)	mt(3·8)	fl		0·34
35	1·49	5·21[g]	1	1947	−6·48	+4·30	gl(24·9)	ol(7·9)	cpx(27·8)	pl(33·2)	mt(4·3)	opx(1·9)	fl	0·32
34	0·89	5·19[g]	1	1947	−6·48	+4·30	gl(17·0)	ol(5·7)	cpx(29·9)	pl(37·4)	mt(4·5)	opx(5·5)	fl	0·25
950° C; 203 MPa; 20 h														
49	4·70	5·19[g]	1	1862	−7·29	+4·28	gl(20·4)	cpx(17·4)	pl(25·8)	mt(3·9)	opx(3·9)	am(28·6)	fl	0·10
48	2·53	5·25[g]	1	1862	−7·29	+4·28	gl(12·6)	cpx(16·7)	pl(35·7)	mt(4·4)	opx(7·1)	am(23·5)	fl	0·21
47[h]	1·49	5·24[g]	1	1862	−7·29 (−7·91)[i]	+4·28	gl(4·8)	cpx(26·0)	pl(44·3)	mt(4·1)	ilm(2·4)	opx(13·9)	am(4·5) fl	
46[h]	0·89	5·24[g]	1	1862	−7·29 (−7·99)	+4·28	gl(4·2)	cpx(26·3)	pl(45·5)	mt(3·1)	ilm(2·9)	opx(13·6)	am(4·4) fl	

[a]H_2O content in pre-hydrated glasses measured by Karl–Fischer titration.
[b]Water content of the residual glass estimated by mass balance calculations (see text).
[c]log f_{O_2} based on equation for MnO–Mn_3O_4 buffer curve (Chou, 1978) assuming intrinsic buffering capacity of IHPV corresponding to the MnO–Mn_3O_4 buffer (see text).
[d]ΔQFM indicates log f_{O_2} (experiment)–log f_{O_2} (QFM buffer) as estimated by Schwab & Küstner (1981).
[e]gl, glass; ol, olivine; cpx, clinopyroxene; opx, orthopyroxene; pl, plagioclase; mt, magnetite; ilm, ilmenite; am, amphibole; fl, fluid (H_2O).
[f]Phase proportions calculated by mass balance are given in wt %.
[g]Runs with $a_{H_2O} = 1$ where water content was calculated using the Burnham model (Burnham, 1979).
[h]Melt composition was calculated using analySIS© (see text).
[i]Log f_{O_2} values in parentheses are calculated using experimentally crystallized coexisting ilm–mt pairs (Andersen *et al.*, 1993).
[j]H_2O added to dry glass powder.
[k]Phases have been identified qualitatively.

Table 3b: Experimental conditions and results for composition B2 (MnO–Mn_3O_4 buffer)

Run	wt % H_2O[a] bulk	wt % H_2O[b] in melt	a_{H_2O}	f_{H_2O} (bar)	log f_{O_2}[c] (bar)	ΔQFM[d] (bar)	Phases and modal proportions[e,f]							ΣR^2
1150°C; 203 MPa; 20·15 h														
86	4·50	4·58[g]	1	2058	−4·38	+4·33	gl(100)	fl						
87	2·05	2·05	0·34	695	−5·33	+3·39	gl(100)	mt(tr)						
88	1·25	1·25	0·15	309	−6·03	+2·69	gl(100)	mt(tr)						
89	0·74	0·75	0·06	127	−6·80	+1·91	gl(98·7)	mt(1·3)						0·32
1100°C; 201 MPa; 21·5 h														
90	4·50	4·63[g]	1	1997	−5·03	+4·32	gl(97·8)	mt(2·2)	fl					0·41
91	2·05	2·10	0·34	688	−5·96	+3·40	gl(97·7)	cpx(1·2)	mt(1·1)					0·52
92	1·25	1·84	0·28	554	−6·15	+3·21	gl(68·1)	cpx(12·5)	pl(16·5)	mt(2·9)				0·21
93	0·74	1·45	0·19	386	−6·46	+2·90	gl(51·0)	cpx(18·5)	pl(27·2)	mt(3·3)				0·45
1050°C; 204 MPa; 20 h														
94	4·50	4·80[g]	1	1992	−5·73	+4·31	gl(92·5)	cpx(2·5)	mt(5·0)	fl				0·61
95	2·05	2·65	0·43	861	−6·45	+3·58	gl(77·5)	cpx(15·7)	mt(6·8)	pl(tr)				0·74
96	1·25	2·48	0·38	765	−6·56 (−6·97)[i]	+3·48	gl(50·5)	cpx(19·8)	opx(1·9)	pl(20·6)	mt(6·5)	ilm(0·7)		0·37
98	0·74	2·22	0·32	644	−6·71 (−7·28)	+3·33	gl(33·2)	cpx(18·9)	opx(4·7)	pl(35·4)	mt(6·7)	ilm(1·1)		0·60
1000°C; 204 MPa; 19·75 h														
99	4·50	5·06[g]	1	1936	−6·48	+4·30	gl(75·1)	cpx(18·3)	mt(6·6)	fl				1·03
100	2·05	5·18[g]	1	1936	−6·48 (−6·91)	+4·30	gl(35·4)	cpx(23·7)	opx(3·0)	pl(30·3)	mt(6·3)	ilm(1·3)	fl	0·52
101	1·25	5·26[g]	1	1936	−6·48 (−7·07)	+4·30	gl(21·8)	cpx(24·4)	opx(5·0)	pl(40·8)	mt(5·4)	ilm(2·6)	fl	0·38
102	0·74	4·23	0·78	1516	−6·69 (−7·58)	+4·08	gl(17·5)	cpx(29·5)	opx(2·4)	pl(42·3)	mt(7·6)	ilm(0·7)		0·75
950°C;201 MPa; 21·5 h														
103	4·50	5·19[g]	1	1848	−7·29 (−7·37)	+4·28	gl(41·5)	cpx(19·1)	pl(19·1)	mt(5·7)	ilm(2·2)	am(14·8)	fl	0·61
104	2·05	5·14[g]	1	1848	−7·29 (−7·76)	+4·28	gl(16·8)	cpx(22·4)	opx(6·0)	pl(45·7)	mt(6·7)	ilm(2·4)	fl	1·04
105	1·25	5·29[g]	1	1848	−7·29 (−7·92)	+4·28	gl(15·5)	cpx(24·1)	opx(7·3)	pl(45·0)	mt(5·5)	ilm(2·6)	fl	0·20
106	0·74	5·20[g]	1	1848	−7·29 (−8·19)	+4·28	gl(14·0)	cpx(28·0)	opx(3·2)	pl(45·4)	mt(6·7)	ilm(2·7)	fl	0·15
950°C; 203 MPa; 96 h														
111	2·05	5·18[g]	1	1863	−7·29 (−7·83)	+4·28	gl(19·1)	cpx(19·2)	opx(6·2)	pl(45·8)	mt(6·9)	ilm(2·8)	fl	0·64

Notes and abbreviations are given below Table 3a.

Table 3c: Experimental conditions and results for composition B1 (QFM buffer)

Run	wt % H_2O[a] bulk	wt % H_2O[b] in melt	a_{H_2O}	f_{H_2O} (bar)	log f_{O_2}[c] (bar)	ΔQFM[d] (bar)	Phases and modal proportions[e,f]							ΣR^2
1150°C; 207 MPa; 2·2 h														
130	6·52[j]	4·58[g]	1	2085	−8·51	+0·20	gl(100)	fl						
129	2·01[j]	2·08	0·33	696	−9·46	−0·75	gl(96·7)	ol(3·3)						0·97
1150°C; 206 MPa; 2 h														
128	0·96[j]	1·02	0·10	215	−10·56	−1·85	gl(94·5)	ol(5·5)						0·76
127	0·35[j]	0·38	0·02	36	−12·12	−3·41	gl(91·9)	ol(5·9)	cpx(0·3)	pl(1·9)				0·83
1100°C; 203 MPa; 3 h														
134	6·41[j]	4·53[g]	1	1998	−9·27	+0·09	gl(95·6)	ol(4·4)	fl					0·45
1100°C; 204 MPa; 3 h														
132	2·00[j]	2·37	0·40	806	−10·15	−0·80	gl(84·4)	ol(7·9)	cpx(4·8)	pl(2·9)				0·68
1100°C; 203 MPa; 3·1 h														
133	1·01[j]	1·49	0·20	398	−10·67	−1·31	gl(67·3)	ol(8·2)	cpx(9·0)	pl(15·5)				0·82
1100°C; 204 MPa; 3·1 h														
131	0·47[j]	0·85	0·07	150	−11·61	−2·26	gl(55·6)	ol(11·2)	cpx(13·7)	pl(19·5)				0·43
1050°C; 207 MPa; 4·5 h														
142	6·36[j]	4·84[g]	1	1999	−10·05	−0·01	gl(80·8)	ol(7·3)	cpx(11·9)	pl(tr)	fl			0·42
141	2·03[j]	3·33	0·64	1289	−10·43	−0·39	gl(60·9)	ol(8·6)	cpx(17·6)	pl(12·9)				0·41
1050°C; 208 MPa; 4·6 h														
140	0·96[j]	2·90	0·51	1024	−10·57	−0·54	gl(33·0)	ol(12·1)	cpx(24·3)	pl(30·6)				0·28
1050°C; 200 MPa; 4·7 h														
143	0·55[j]	2·04	0·32	616	−10·95	−0·91	gl(27·2)	ol(12·6)	cpx(26·2)	pl(34·0)				0·35
1000°C; 207 MPa; 9·2 h														
148	4·46	5·06[g]	1	1947	−10·76	+0·01	gl(48·8)	ol(11·4)	cpx(24·2)	pl(15·6)	fl			0·13
1000°C; 207 MPa; 5·5 h														
147	1·91	5·01	0·99	1921	−10·76	+0·02	gl(38·2)	ol(11·5)	cpx(26·3)	pl(24·0)				0·19
146	1·12	5·04	0·99	1946	−10·74	+0·03	gl(20·2)	ol(12·0)	cpx(31·8)	pl(35·9)				0·28
145	0·55	3·52	0·64	1248	−11·13	−0·36	gl(14·5)	ol(14·5)	cpx(29·1)	pl(40·7)				0·40
950°C; 206 MPa; 7·5 h														
153	4·46	5·12[g]	1	1879	−11·48	+0·09	gl(18·5)	ol(4·9)	cpx(25·8)	pl(28·5)	am(22·3)	fl		0·56
152	1·91	5·12[g]	1	1879	−11·48	+0·09	gl(14·2)	ol(8·2)	cpx(23·3)	pl(35·9)	am(18·4)	fl		0·31
151	1·12	5·17[g]	1	1879	−11·48	+0·09	gl(7·9)	ol(8·1)	cpx(29·1)	pl(36·6)	am(17·3)	ilm(1·0)	fl	0·16
150	0·55	—	—	1879	−11·48	+0·09	ol[k]	cpx[k]	pl[k]	am[k]	ilm[k]			

Notes and abbreviations are given below Table 3a.

calculated melt Fe^{2+}/Fe^{3+} ratios were not corrected with respect to the melt water content, because the data of Baker & Rutherford (1996) and Gaillard *et al.* (2001) were obtained for water-saturated conditions in very silicic melts only. Thus, the effect of dissolved H_2O on the Fe^{2+}/Fe^{3+} ratio in basaltic melts, especially in runs at $a_{H_2O} < 1$, is unknown.

Analytical techniques and determination of phase proportions

Electron microprobe analyses of glasses and minerals were performed with a Cameca Camebax and a Cameca SX 100 instrument and are listed in Table 4. Analytical conditions for minerals were 15 kV, 15 nA beam current, and counting times of 5 s for Na and K, and 10 s for all other elements. Glasses were analysed with a defocused beam of 20 μm with a 5 nA beam current and counting times of 2 s for Na and K, and 5 s for the other elements. In crystal-rich runs (glass < 30 wt %) the beam was defocused as much as possible, but loss of alkalis was observed for spot sizes <15 μm. In this case analyses were corrected by a loss factor using the B1 hydrous starting glasses as standards with known water contents.

Phase proportions (wt %) were determined by mass balance (glass analyses were normalized to 100 wt %). Melt water contents in runs with $a_{H_2O} < 1$ were calculated using the known melt fractions and bulk water content of the starting materials. No attempts were made to consider the water content in amphiboles, because runs within the amphibole stability field (Table 3; see Fig. 4) were water saturated.

The melt water content was also estimated for all runs with the 'by-difference' method (Devine *et al.*, 1995; Koepke, 1997). Comparison of melt water contents obtained by mass balance ($a_{H_2O} < 1$) and from the 'Burnham model' ($a_{H_2O} = 1$) with the water contents determined with the 'by-difference' method show good agreement (Fig. 2).

In experiments with low melt fractions, in which water-saturated conditions mostly prevailed, melt water contents obtained by the 'by-difference' method were relatively higher than those from the 'Burnham model' (see triangles in Fig. 2 for runs with $a_{H_2O} = 1$). This is probably due to too low microprobe totals resulting from analyses of very small melt pools with a beam that could not be defocused. Analyses of glasses in runs with low melt fractions were possible because small batches of crystal-free residual liquid were located along the capsule rim. This was especially the case for run 151 containing about 8 wt % melt. However, for the near-solidus experiments 47 and 46 the remaining glass pools were too small to be analysed even with a focused beam. Hence, phase proportions (vol. %) have been estimated from back-scattered electron (BSE) images using analySIS© 3.0 software (Gardien *et al.*, 1995; Koepke *et al.*, 1996). The proportion in wt % (Table 3a) was recalculated assuming typical average densities for the solid phases and for the melt (melt density of 2·28 g/cm^3 is estimated from glass composition of run 48 after Lange (1997), Lange & Carmichael (1990) and Ochs & Lange (1999)]. For these two experiments the melt compositions were roughly determined by mass balance calculations.

Experimental limitations and general aspects on the effect of H_2O on experimental results

It should be emphasized that there are different ways to understand the effect of H_2O on mineral compositions and liquid lines of descent. The effect of bulk water content can be estimated by comparing experimental charges obtained at identical temperature with different bulk water content of the charge. However, comparison of such experiments shows that the crystal amount is not the same at different bulk water contents, especially for high-temperature runs (e.g. runs 42–45 at 1100°C; Table 3a; Fig. 3a). In these high-temperature experiments, residual melts have different water contents and therefore different a_{H_2O}. In contrast, for low-temperature runs (e.g. runs 34–37 at 1000°C, Table 3a) the crystal content is always high enough to attain fluid-saturated conditions (as a result of crystallization of mostly anhydrous phases). Thus, at high temperatures, a decrease of the bulk water content results in a strong decrease of a_{H_2O} in the experimental charge. In contrast, at low temperature, only small changes in a_{H_2O} with changing bulk water content are expected. In subsequent sections, results are discussed as a function of either bulk water content or a_{H_2O}. It is emphasized that these two parameters are not identical.

From the discussion above, it could be expected that, at low temperatures (e.g. 950 and 1000°C), experimental conditions are always fluid saturated (water saturated), and all other parameters being equal (P, T, bulk composition, f_{O_2}), the phase assemblage and composition should be identical. The results in Fig. 4 show that this is not the case because the melt proportion, the relative proportions of minerals and, therefore, melt composition (see Figs 9–11) differ as a function of the bulk water content. An additional possible explanation is that despite the presence of a free fluid phase in these runs (Table 3) a_{H_2O} may be decreased by the presence of air in the capsules. Thus, a_{H_2O} slightly decreases with decreasing bulk water content because of the higher N_2/H_2O ratio in experiments with starting glasses containing low water contents. The X_{H_2O} [defined as $X_{H_2O}/(X_{H_2O} + X_{N_2})$] in these charges was estimated to be 0·92 (for lowest bulk water contents). The small changes in a_{H_2O} for given bulk water contents at low temperature influence both composition

Table 4a: Electron microprobe analyses of run products for composition B1 (MnO–Mn_3O_4 buffer conditions)

Run	Phase	*n*	SiO_2	TiO_2	Al_2O_3	FeO*[a]	MnO	MgO	CaO	Na_2O	K_2O	P_2O_5	Total	X_{Ph}[b]	K_d[c]
66	gl	6	49·67(20)[d]	0·85(9)	16·01(21)	8·59(9)	0·14(8)	9·83(10)	12·39(21)	2·33(19)	0·10(8)	0·09(9)	94·80(76)	82·66	
65	gl	3	49·88(1·12)	0·77(12)	16·29(30)	9·06(75)	0·10(9)	9·21(8)	12·41(12)	2·20(24)	0·03(1)	0·04(2)	97·88(89)	78·15	
	ol	4	41·48(21)	0·04(2)	0·04(2)	8·41(5)	0·15(2)	50·45(15)	0·33(8)	0·02(8)	0·01(0)		100·93	91·45	0·334
64	gl	3	50·19(19)	0·86(10)	16·72(20)	8·51(19)	0·17(3)	8·41(7)	12·77(6)	2·27(5)	0·07(5)	0·03(3)	98·89(62)	75·31	
	ol	5	41·24(31)	0·02(2)	0·05(3)	10·00(22)	0·18(4)	49·08(12)	0·34(4)	0·01(0)	0·01(1)		100·93	89·74	0·349
63	gl	6	50·34(45)	0·93(16)	16·58(18)	8·79(28)	0·15(17)	8·00(19)	12·5(17)	2·51(25)	0·11(7)	0·05(9)	98·78(75)	71·59	
	ol	4	41·35(22)	0·01(2)	0·05(4)	11·26(9)	0·20(5)	48·07(15)	0·41(3)	0·01(1)	0·01(1)		101·39	88·38	0·331
	cpx	4	51·67(31)	0·47(9)	4·50(15)	6·11(38)	0·18(5)	16·84(14)	21·11(56)	0·25(3)	0·01(1)		101·14	47/10/43	0·318
	pl	4	49·37(98)	0·10(2)	30·90(50)	1·39(19)	0·02(2)	0·80(20)	16·12(67)	2·39(36)	0·02(0)		101·12	78·7	1·35
45	gl	4	50·15(74)	0·82(6)	16·29(35)	8·69(29)	0·17(5)	8·97(18)	12·47(40)	2·26(28)	0·11(5)	0·08(9)	94·98(76)	81·31	
	ol	8	41·49(20)	0·03(2)	0·04(2)	6·72(18)	0·21(5)	51·34(40)	0·23(2)	0·01(1)	0·01(1)		100·07	93·16	0·319
44	gl	6	50·16(47)	0·91(14)	17·42(40)	9·47(34)	0·21(2)	7·12(14)	11·95(20)	2·58(32)	0·09(6)	0·09(8)	96·79(98)	73·73	
	ol	6	40·82(11)	0·02(1)	0·08(3)	10·14(21)	0·22(8)	48·83(60)	0·33(4)	0·01(1)	0·01(1)		100·45	89·68	0·327
	cpx	4	48·08(32)	0·55(8)	6·70(16)	7·61(26)	0·09(4)	14·74(18)	21·73(14)	0·27(4)	0·00(1)		99·77	43/12/45	0·269
	pl	5	46·42(56)	0·12(6)	31·47(1·07)	1·85(52)	0·01(1)	0·82(50)	17·05(41)	1·63(8)	0·02(1)		99·39	85·2	2·26
43	gl	4	50·96(53)	1·25(10)	17·12(80)	10·19(73)	0·14(13)	6·12(17)	11·22(29)	2·64(16)	0·14(2)	0·22(14)	97·43(1·11)	67·39	
	ol	6	40·18(23)	0·02(2)	0·10(8)	13·13(19)	0·29(5)	44·89(73)	0·36(3)	0·02(1)	0·01(1)		99·00	85·90	0·339
	cpx	5	49·09(62)	0·63(3)	5·76(58)	7·79(37)	0·15(5)	14·71(49)	20·84(40)	0·37(6)	0·01(1)		99·35	43/13/44	0·351
	pl	4	49·29(1·50)	0·06(2)	30·63(24)	1·36(27)	0·05(3)	0·41(16)	15·32(79)	2·72(54)	0·02(1)		99·85	75·6	1·33
42	gl	10	51·38(57)	1·46(11)	15·97(57)	10·98(25)	0·19(15)	6·16(29)	10·50(30)	3·06(24)	0·12(7)	0·18(12)	97·54(96)	64·00	
	ol	7	39·98(24)	0·03(4)	0·08(11)	14·68(14)	0·29(2)	43·64(42)	0·36(4)	0·01(1)	0·00(0)		99·09	84·12	0·335
	cpx	5	49·29(39)	0·61(5)	5·28(28)	8·16(30)	0·19(4)	15·13(23)	20·40(30)	0·36(3)	0·01(1)		99·43	44/14/42	0·294
	pl	6	49·67(56)	0·08(5)	29·93(81)	1·56(2)	0·04(3)	0·45(19)	14·94(43)	2·87(27)	0·03(1)		99·56	74·1	1·52
62	gl	3	49·79(4)	0·82(6)	16·07(21)	8·84(4)	0·19(2)	9·10(7)	12·79(17)	2·11(6)	0·12(3)	0·17(7)	95·15(70)	81·31	
	ol	3	41·24(23)	0·03(1)	0·05(2)	6·71(14)	0·31(7)	51·44(14)	0·24(3)	0·00(1)	0·00(0)		100·03	93·39	0·318
61	gl	3	51·35(65)	1·34(3)	16·28(52)	10·68(14)	0·16(7)	6·20(22)	10·54(37)	3·16(32)	0·13(8)	0·15(9)	97·92(61)	64·51	
	ol	2	40·12(4)	0·06(4)	0·14(17)	14·69(28)	0·37(9)	43·66(21)	0·35(8)	0·01(1)	0·01(1)		99·40	84·12	0·343
	cpx	2	49·38(25)	0·60(1)	5·28(34)	8·17(19)	0·20(1)	15·28(8)	20·30(25)	0·35(4)	0·01(1)		99·55	44/14/42	0·301
	pl	3	49·95(8)	0·17(6)	29·87(20)	1·34(11)	0·01(1)	0·43(2)	15·02(7)	2·70(2)	0·02(1)		99·48	75·4	1·67
41	gl	2	51·13(33)	0·98(5)	18·17(10)	8·62(46)	0·24(14)	6·03(4)	12·19(8)	2·43(18)	0·07(1)	0·15(9)	94·16(98)	74·76	
	ol	3	41·19(6)	0·02(3)	0·04(3)	9·90(14)	0·30(9)	46·70(52)	0·19(3)	0·02(2)	0·01(1)		98·37	89·37	0·338
	cpx	3	49·49(58)	0·64(18)	5·88(33)	6·75(5)	0·28(3)	15·20(56)	21·22(46)	0·32(5)	0·00(0)		99·77	44/11/45	0·408
	pl	3	46·39(4)	0·06(3)	33·55(15)	1·18(6)	0·04(5)	0·18(3)	18·24(33)	1·41(4)	0·01(0)		101·04	87·7	2·58
	mt	2	0·49(20)	2·47(2)	7·20(74)	57·56/22·19	0·38(6)	7·49(20)	0·45(11)	0·02(2)	0·00(1)		98·22	7·26	

Table 4a: Continued

Run	Phase	*n*	SiO_2	TiO_2	Al_2O_3	FeO*[a]	MnO	MgO	CaO	Na_2O	K_2O	P_2O_5	Total	X_{Ph}[b]	K_d[c]
40	gl	6	53·43(83)	0·95(13)	18·40(1·15)	8·77(66)	0·20(14)	4·63(17)	10·37(65)	2·99(25)	0·11(5)	0·15(8)	94·89(45)	68·66	
	ol	6	40·44(25)	0·02(1)	0·05(3)	11·92(21)	0·31(4)	44·76(63)	0·29(5)	0·01(1)	0·01(0)		97·81	87·00	0·327
	cpx	3	51·36(24)	0·46(21)	4·01(35)	6·40(1)	0·19(5)	15·18(0)	21·97(51)	0·29(6)	0·01(0)		99·86	44/11/45	0·411
	pl	2	48·06(2)	0·19(5)	30·53(77)	2·07(30)	0·06(2)	0·76(21)	16·36(32)	1·81(4)	0·04(2)		99·88	83·1	2·60
	mt	2	0·21(5)	2·45(70)	8·48(1·16)	56·33/22·41	0·30(2)	7·15(34)	0·37(3)	0·04(2)	0·01(1)		97·75	7·49	
39	gl	5	53·64(1·53)	1·24(11)	17·82(1·51)	9·34(42)	0·21(5)	4·24(19)	9·73(96)	3·47(28)	0·23(6)	0·08(6)	96·24(1·11)	63·70	
	ol	2	40·13(23)	0·05(6)	0·35(30)	14·24(24)	0·32(4)	45·13(62)	0·32(0)	0·05(1)	0·00(0)		100·61	84·96	0·311
	cpx	3	49·36(70)	0·76(7)	5·18(36)	7·89(11)	0·25(1)	15·59(26)	20·16(24)	0·36(6)	0·00(0)		99·55	45/13/42	0·261
	pl	3	49·52(43)	0·15(4)	29·58(84)	1·58(13)	0·00(0)	0·56(14)	14·32(64)	3·00(10)	0·04(1)		98·76	72·4	1·70
	mt	2	0·16(2)	3·67(75)	6·48(41)	56·79/24·51	0·29(3)	6·56(31)	0·36(4)	0·02(4)	0·00(0)		98·83	10·99	
38	gl	2	54·54(1·21)	1·32(19)	18·17(70)	8·82(76)	0·23(8)	4·27(39)	8·79(83)	3·46(89)	0·24(6)	0·15(11)	96·95(1·28)	62·05	
	ol	2	39·75(11)	0·02(2)	0·08(3)	15·60(28)	0·41(6)	43·40(47)	0·32(3)	0·05(2)	0·01(1)		99·63	83·22	0·330
	cpx	5	49·53(46)	0·87(15)	5·74(29)	8·58(87)	0·20(3)	15·09(10)	18·89(4)	0·39(9)	0·01(1)		99·30	45/15/40	0·418
	pl	2	50·70(87)	0·11(2)	30·01(34)	1·30(18)	0·01(1)	0·45(12)	14·25(11)	3·14(9)	0·04(0)		100·00	71·3	1·79
	mt	3	0·14(3)	4·94(15)	6·72(52)	52·09/25·51	0·30(7)	6·04(6)	0·34(5)	0·06(5)	0·00(0)		96·15	15·47	
37	gl	3	56·17(83)	1·05(11)	18·79(33)	6·50(27)	0·13(14)	4·47(7)	8·76(29)	3·74(67)	0·14(9)	0·24(2)	94·53(1·50)	74·69	
	ol	2	41·16(10)	0·03(4)	0·07(4)	9·66(68)	0·33(8)	49·16(91)	0·20(5)	0·01(1)	0·01(0)		100·61	90·07	0·325
	cpx	2	48·57(4)	0·76(3)	6·19(6)	7·54(17)	0·19(4)	15·63(23)	20·50(49)	0·32(0)	0·01(1)		99·70	45/13/42	0·311
	pl	3	46·33(2)	0·00(3)	32·90(15)	1·25(4)	0·04(2)	0·19(4)	17·41(9)	1·68(11)	0·04(3)		99·83	84·9	4·43
	mt	2	0·25(16)	2·49(6)	7·13(4)	58·66/21·51	0·38(4)	7·84(9)	0·40(13)	0·01(1)	0·01(1)		98·69	7·20	
	am	3	42·66(29)	1·77(3)	12·48(28)	8·21(20)	0·13(7)	17·71(6)	11·72(21)	2·44(4)	0·04(2)		97·15	85·7	
36	gl	4	57·57(55)	1·07(1)	18·04(41)	6·82(42)	0·12(4)	3·88(28)	8·05(14)	3·84(23)	0·29(4)	0·33(17)	94·74(1·95)	70·84	
	ol	2	40·90(41)	0·04(2)	0·24(28)	11·61(1)	0·31(0)	46·86(72)	0·24(4)	0·04(3)	0·01(1)		100·24	87·80	0·338
	cpx	3	49·27(15)	0·86(3)	5·15(29)	7·41(81)	0·25(2)	15·66(42)	20·58(1·28)	0·34(6)	0·00(0)		99·52	45/12/43	0·308
	pl	3	49·12(30)	0·24(12)	29·43(1·35)	1·93(31)	0·02(1)	1·00(45)	15·19(57)	2·10(10)	0·03(0)		99·06	79·8	3·46
	mt	2	0·22(8)	3·27(7)	6·06(7)	57·12/22·97	0·38(2)	6·96(2)	0·41(0)	0·01(1)	0·01(1)		97·42	9·66	
35	gl	4	57·53(59)	1·00(12)	19·24(1·43)	6·43(68)	0·16(12)	2·99(27)	7·74(84)	4·39(29)	0·26(7)	0·26(10)	93·85(1·13)	66·63	
	ol	3	41·07(13)	0·04(1)	0·25(26)	13·15(17)	0·38(5)	44·37(38)	0·23(4)	0·03(3)	0·01(1)		99·53	85·74	0·332
	cpx	2	50·46(73)	0·93(18)	4·47(50)	7·15(42)	0·30(7)	15·67(47)	20·19(53)	0·40(1)	0·00(0)		99·57	46/12/42	0·372
	pl	3	51·05(44)	0·13(11)	29·09(1·60)	1·51(49)	0·02(3)	0·72(64)	14·33(14)	3·01(30)	0·03(1)		99·90	72·3	2·70
	mt	1	0·20	4·35	5·58	54·98/24·94	0·31	6·31	0·34	0·00	0·00		97·00	13·18	
	opx	2	54·63(62)	0·34(8)	3·17(60)	9·99(3)	0·33(1)	29·32(54)	2·00(40)	0·05(1)	0·00(0)		99·84	80/16/4	

Run	Phase	*n*	SiO_2	TiO_2	Al_2O_3	FeO*[a]	MnO	MgO	CaO	Na_2O	K_2O	P_2O_5	Total	X_{Ph}[b]	K_d[c]
34	gl	3	58·68(66)	1·35(13)	18·12(58)	6·36(6)	0·27(6)	2·70(22)	7·09(35)	4·91(42)	0·24(13)	0·27(7)	93·13(1·65)	64·96	
	ol	2	40·89(0)	0·04(0)	0·60(60)	13·10(23)	0·37(9)	43·34(1·25)	0·19(4)	0·06(3)	0·01(1)		98·61	85·50	0·314
	cpx	3	50·10(40)	1·00(3)	4·51(43)	7·83(66)	0·23(8)	15·70(23)	19·72(29)	0·42(4)	0·00(1)		99·51	46/13/41	0·356
	pl	2	51·55(52)	0·13(6)	29·61(42)	1·30(17)	0·04(5)	0·50(27)	13·67(2)	3·24(10)	0·03(0)		100·08	69·9	2·93
	mt	2	0·14(10)	4·94(3)	5·49(20)	53·91/25·09	0·32(2)	6·30(14)	0·30(11)	0·04(0)	0·02(1)		96·55	15·00	
	opx	5	53·94(1·08)	0·40(7)	3·35(77)	9·98(34)	0·34(6)	28·87(72)	1·82(25)	0·09(4)	0·01(1)		98·80	80/16/4	
49	gl	4	63·16(96)	0·70(6)	16·75(50)	5·31(38)	0·12(13)	2·52(30)	6·43(33)	4·45(66)	0·29(10)	0·25(25)	92·94(1·49)	67·83	
	cpx	3	51·13(1·32)	0·67(7)	5·10(16)	7·12(35)	0·28(5)	15·84(26)	20·50(16)	0·35(6)	0·01(1)		100·99	46/12/42	0·397
	pl	4	49·84(19)	0·05(4)	31·36(64)	1·32(10)	0·02(1)	0·38(15)	15·97(23)	2·36(18)	0·02(1)		101·33	78·8	4·69
	mt	4	0·28(3)	2·17(12)	4·94(1)	60·52/23·25	0·38(5)	6·22(5)	0·37(5)	0·01(1)	0·00(0)		98·14	6·07	
	opx	3	55·40(32)	0·24(2)	3·50(35)	8·35(29)	0·35(5)	30·81(54)	1·60(27)	0·21(30)	0·05(7)		100·52	84/13/3	
	am	6	44·71(37)	1·65(12)	11·60(26)	9·00(48)	0·17(7)	17·15(10)	11·65(21)	2·24(6)	0·05(1)		98·23	82·5	
48	gl	3	63·49(1·73)	0·86(10)	17·21(1·12)	5·24(21)	0·30(2)	1·82(34)	6·20(13)	4·78(67)	0·23(4)	0·15(3)	93·05(1·28)	60·82	
	cpx	2	51·57(41)	0·72(2)	4·62(15)	7·19(12)	0·27(4)	15·75(33)	20·89(21)	0·45(9)	0·00(0)		101·46	45/12/43	0·284
	pl	2	51·57(38)	0·22(6)	27·59(1·13)	1·76(17)	0·03(3)	1·78(55)	14·65(42)	2·51(7)	0·04(1)		100·16	76·2	4·50
	mt	3	0·89(58)	2·84(1·47)	4·99(76)	57·12/23·86	0·36(0)	6·23(29)	0·55(25)	0·07(7)	0·01(0)		96·91	8·42	
	opx	2	55·52(18)	0·31(2)	3·20(10)	8·55(8)	0·47(9)	30·01(54)	1·71(18)	0·08(0)	0·01(1)		99·86	83/14/3	
	am	3	45·08(82)	1·92(41)	11·85(69)	9·19(58)	0·19(2)	16·14(74)	11·70(5)	2·33(6)	0·06(1)		98·47	79·2	
47	gl	—	63·73	1·00	16·43	5·75	0·02	1·35	5·78	5·48	0·34	0·15	—	51·26	
	cpx	3	52·37(9)	0·62(4)	4·53(4)	5·57(3)	0·28(5)	14·92(14)	20·58(13)	0·43(3)	0·03(1)		99·32	45/10/45	0·223
	pl	2	52·31(16)	0·22(4)	28·51(2)	1·20(2)	0·00(0)	1·23(3)	13·35(6)	3·53(3)	0·05(3)		100·41	67·4	3·58
	mt	2	0·15(21)	3·80(34)	5·82(3·18)	55·53/23·94	0·36(9)	5·95(1·83)	0·32(21)	0·16(5)	0·01(0)		96·04	11·53	
	ilm	1	1·18	19·49	1·46	58·89/11·56	0·22	3·41	0·62	0·06			96·89	31·49	
	opx	3	55·43(5)	0·25(2)	3·02(1)	9·17(2)	0·41(1)	29·22(2)	1·60(2)	0·04(0)	0·02(1)		99·17	82/15/3	
	am	2	44·05(24)	2·09(34)	12·56(55)	8·96(50)	0·15(9)	15·33(31)	11·62(48)	2·42(12)	0·07(2)		97·23	78	
46	gl	—	64·16	1·15	15·86	5·70	0·22	1·29	5·49	5·54	0·39	0·21	—	50·76	
	cpx	2	52·39(91)	0·61(11)	4·60(9)	5·49(12)	0·25(6)	14·99(27)	20·70(17)	0·41(5)	0·03(1)		99·47	45/10/45	0·212
	pl	3	53·39(17)	0·14(8)	28·31(51)	1·30(11)	0·01(0)	0·30(5)	13·01(37)	3·71(11)	0·05(2)		100·22	65·8	3·54
	mt	1	0·17	4·58	5·82	53·85/25·00	0·39	6·09	0·34	0·04	0·01		96·29	14·01	
	ilm	1	1·16	20·32	1·33	57·83/13·09	0·23	2·99	0·55	0·06	0·01		97·56	34·24	
	opx	2	55·44(33)	0·25(8)	2·99(29)	9·30(13)	0·45(1)	29·99(44)	1·60(19)	0·04(3)	0·03(1)		100·09	82/15/3	
	am	3	44·02(51)	2·12(23)	12·39(37)	9·04(21)	0·17(2)	15·41(47)	11·70(31)	2·37(11)	0·06(3)		97·28	77·9	

[a]Fe concentrations are given as FeO* (total iron), except for magnetite and ilmenite, where Fe is given as Fe_2O_3/FeO contents.
[b]Numbers represent: Mg-number for glass defined as MgO/(MgO + FeO) × 100 and FeO and Fe_2O_3 content calculated after Kress & Carmichael (1991); $X_{Fo} \times 100$ for olivine; En/Fs/Wo content for pyroxene; An content for plagioclase; $X_{Mt} \times 100$ for magnetite and $X_{Ilm} \times 100$ for ilmenite; Mg-number for amphibole defined as $X_{Mg}/(X_{Mg} + X_{Fe^{2+}}) \times 100$.
[c]Numbers represent partition coefficients, defined as $(X_{FeO-Ol}/X_{FeO-Liq} \times X_{MgO-Liq}/X_{MgO-Ol})$ for olivine, $(X_{FeO-Cpx}/X_{MgO-Cpx} \times X_{MgO-Liq}/X_{FeO-Liq})$ for clinopyroxene, and $(X_{CaO-Plag}/X_{Na_2O-Plag} \times X_{Na_2O-Liq}/X_{CaO-Liq})$ for plagioclase.
[d]Numbers in parentheses are one standard deviation of replicate analyses in terms of least units cited.

Table 4b: Electron microprobe analyses of run products for composition B2 (MnO–Mn_3O_4 buffer conditions)

Run	Phase	*n*	SiO_2	TiO_2	Al_2O_3	FeO*[a]	MnO	MgO	CaO	Na_2O	K_2O	P_2O_5	Total	X_{Ph}[b]	K_d[c]
86	gl	10	51·17(23)	1·43(6)	15·93(16)	10·72(26)	0·21(7)	6·49(7)	10·57(13)	3·13(11)	0·15(4)	0·19(7)	94·89(38)	71·11	
87	gl	3	50·91(61)	1·51(5)	15·68(24)	11·46(47)	0·31(13)	6·40(18)	10·39(13)	3·15(13)	0·06(2)	0·12(3)	97·85(75)	64·49	
88	gl	4	51·43(27)	1·49(13)	15·80(29)	10·47(43)	0·29(20)	6·38(21)	10·60(15)	3·36(16)	0·09(2)	0·08(4)	98·09	63·78	
89	gl	8	51·71(29)	1·41(8)	15·90(24)	10·45(72)	0·23(8)	6·39(12)	10·54(17)	2·96(29)	0·14(6)	0·26(14)	99·20(46)	60·91	
90	gl	2	52·24(74)	1·41(3)	16·14(44)	9·22(50)	0·31(13)	6·19(30)	11·07(4)	3·12(12)	0·16(4)	0·13(6)	94·19(60)	73·98	
	mt	3	0·13(2)	1·54(3)	4·85(1)	63·02/19·84	0·35(1)	7·91(7)	0·36(5)	0·01(1)	0·01(2)		98·02	4·08	
91	gl	4	52·00(62)	1·61(2)	15·80(40)	10·26(54)	0·34(7)	6·22(28)	10·36(44)	3·21(26)	0·09(3)	0·12(4)	97·85(50)	66·62	
	cpx	2	48·42(94)	1·06(4)	5·61(68)	8·98(1)	0·27(1)	14·65(59)	20·12(64)	0·45(3)	0·02(1)		99·58	43/15/42	0·348
	mt	2	0·22(4)	2·83(8)	7·35(5)	56·95/22·97	0·25(6)	7·01(12)	0·37(1)	0·03(1)	0·01(1)		97·99	8·62	
92	gl	4	52·85(7)	1·70(8)	15·35(32)	10·73(21)	0·33(12)	5·91(14)	9·13(18)	3·66(13)	0·18(5)	0·15(3)	98·04(1·03)	63·71	
	cpx	2	51·11(20)	0·73(4)	3·87(62)	8·21(6)	0·30(5)	17·01(87)	17·78(56)	0·42(5)	0·02(2)		99·45	49/14/37	0·369
	pl	2	52·75(93)	0·11(2)	28·49(28)	1·43(9)	0·03(3)	0·28(6)	12·87(35)	4·05(11)	0·04(3)		100·04	63·5	1·27
	mt	2	0·96(75)	4·46(8)	6·59(11)	52·36/26·23	0·24(0)	6·19(13)	0·76(37)	0·00(0)	0·00(0)		97·80	14·17	
93	gl	3	53·08(30)	2·02(11)	14·74(26)	11·94(21)	0·28(13)	5·32(24)	8·85(24)	3·43(28)	0·22(2)	0·14(1)	97·84(31)	56·86	
	cpx	2	51·21(54)	0·82(3)	3·82(9)	9·78(5)	0·35(3)	16·98(7)	16·66(63)	0·42(2)	0·01(2)		100·05	49/16/35	0·348
	pl	2	53·79(29)	0·24(20)	27·04(1·13)	1·70(55)	0·01(2)	0·50(40)	11·80(32)	4·62(6)	0·05(1)		99·75	58·3	0·99
	mt	3	0·27(7)	5·49(44)	6·21(27)	51·67/27·25	0·28(4)	5·59(8)	0·40(5)	0·01(1)	0·02(1)		97·20	17·10	
94	gl	3	54·32(64)	1·49(14)	16·36(52)	7·46(46)	0·15(6)	5·88(15)	10·74(21)	3·31(20)	0·17(4)	0·13(6)	93·81(90)	77·43	
	cpx	2	47·92(97)	1·12(7)	5·54(29)	8·20(7)	0·18(7)	14·07(7)	22·64(7)	0·37(6)	0·01(1)		100·05	40/13/47	0·311
	mt	2	0·18(1)	1·96(4)	4·85(14)	62·55/19·27	0·41(2)	8·53(20)	0·32(7)	0·02(3)	0·02(1)		98·10	5·24	
95	gl	3	56·85(73)	1·38(13)	17·85(2·19)	5·99(41)	0·30(12)	4·17(36)	9·16(1)	3·94(3)	0·28(16)	0·09(4)	97·25(75)	71·59	
	cpx	4	48·34(48)	1·25(25)	5·39(27)	7·78(47)	0·28(3)	15·21(29)	20·48(19)	0·46(6)	0·00(0)		99·19	44/13/43	0·291
	mt	3	0·73(35)	3·93(21)	5·88(32)	56·10/24·01	0·43(5)	7·08(4)	0·55(18)	0·06(7)	0·02(1)		98·80	11·61	
96	gl	5	59·03(71)	1·19(26)	17·96(2·23)	5·74(74)	0·23(22)	3·70(32)	7·72(77)	4·05(11)	0·27(11)	0·09(9)	97·18(1·08)	69·08	
	cpx	5	49·91(48)	0·99(10)	4·75(2·17)	8·06(15)	0·41(3)	15·16(1·35)	19·93(55)	0·59(18)	0·02(3)		99·82	44/14/42	0·398
	opx	3	53·56(6)	0·49(3)	4·02(1·60)	10·92(49)	0·44(7)	27·35(1·50)	2·29(62)	0·24(15)	0·01(1)		99·34	77/18/5	
	pl	3	53·66(38)	0·42(10)	24·51(92)	2·01(69)	0·03(3)	1·65(51)	11·57(77)	4·05(37)	0·08(4)		97·99	60·9	1·50
	mt	2	0·43(1)	5·85(0)	4·34(17)	53·87/27·36	0·46(4)	5·67(5)	0·45(7)	0·05(7)	0·01(1)		98·48	17·18	
	ilm	1	0·69	22·51	1·32	53·87/13·50	0·25	3·67	0·48	0·03	0·00		96·32	37·21	
98	gl	4	59·73(1·23)	0·90(23)	17·92(1·08)	5·56(53)	0·09(2)	3·19(31)	7·58(42)	4·54(57)	0·34(21)	0·15(0)	97·60(1·49)	66·15	
	cpx	3	49·83(47)	0·87(13)	3·73(81)	7·42(49)	0·47(1)	15·75(22)	19·43(78)	0·41(20)	0·03(0)		97·94	46/13/41	0·342
	opx	2	55·62(77)	0·46(8)	1·98(43)	12·37(57)	0·62(13)	26·97(8)	2·70(17)	0·16(1)	0·01(1)		100·89	75/20/5	
	pl	3	54·17(30)	0·10(12)	24·44(1·83)	2·60(59)	0·07(2)	1·83(92)	11·22(69)	4·40(13)	0·10(2)		98·93	58·1	1·53
	mt	3	0·12(1)	6·57(16)	3·87(3)	52·37/28·73	0·46(1)	4·89(3)	0·30(4)	0·01(0)	0·01(0)		97·34	19·41	
	ilm	1	0·48	24·90	1·08	50·83/16·10	0·22	3·33	0·52	0·01	0·00		97·47	42·72	

Run	Phase	*n*	SiO_2	TiO_2	Al_2O_3	FeO*[a]	MnO	MgO	CaO	Na_2O	K_2O	P_2O_5	Total	X_{Ph}[b]	K_d[c]
99	gl	3	56·70(20)	1·42(8)	18·42(64)	5·82(89)	0·14(5)	4·21(7)	9·30(15)	3·67(41)	0·24(6)	0·08(3)	93·71(34)	75·99	
	cpx	4	48·22(65)	1·43(11)	6·76(20)	6·59(74)	0·26(4)	14·26(28)	22·71(38)	0·41(4)	0·01(3)		100·63	41/11/48	0·283
	mt	2	0·22(4)	2·44(4)	5·91(2)	59·71/19·63	0·56(11)	8·46(6)	0·43(2)	0·02(1)	0·01(1)		97·38	6·64	
100	gl	3	60·57(91)	1·12(4)	17·96(57)	5·94(22)	0·39(8)	2·30(27)	6·84(49)	4·32(53)	0·36(5)	0·21(6)	95·28(77)	62·38	
	cpx	4	49·66(47)	1·36(19)	4·68(1·04)	8·26(73)	0·41(2)	16·27(1·25)	17·95(98)	0·51(13)	0·01(0)		99·13	48/14/38	0·332
	opx	2	54·89(18)	0·39(3)	2·99(5)	8·69(17)	0·55(7)	30·31(8)	1·75(16)	0·06(1)	0·00(0)		99·64	82/14/4	
	pl	3	53·45(71)	0·29(9)	26·24(2·07)	1·84(46)	0·01(1)	0·98(60)	12·08(80)	3·71(6)	0·08(2)		98·68	64·0	2·06
	mt	2	0·21(11)	3·44(7)	4·50(4)	58·97/24·06	0·52(4)	6·30(6)	0·35(10)	0·02(2)	0·01(0)		98·38	9·64	
	ilm	2	0·18	18·63	1·26	61·89/10·15	0·25	3·27	0·43	0·04	0·01		96·09	29·51	
101	gl	4	62·17(69)	1·23(4)	17·94(1·02)	5·32(56)	0·25(29)	1·93(4)	5·67(19)	4·89(68)	0·32(8)	0·28(1)	94·41(1·03)	60·85	
	cpx	4	51·03(34)	0·87(14)	3·28(19)	8·30(52)	0·54(7)	16·37(2)	18·96(55)	0·47(1)	0·01(1)		99·82	47/14/39	0·298
	opx	2	54·33(13)	0·31(0)	3·34(74)	10·25(33)	0·56(3)	27·98(1·47)	2·10(69)	0·21(22)	0·01(2)		99·10	79/17/4	
	pl	2	54·60(1·76)	0·21(2)	26·19(95)	2·33(38)	0·02(2)	0·48(22)	10·90(46)	4·44(35)	0·09(6)		99·25	57·3	2·12
	mt	3	0·18(12)	3·72(9)	3·56(2)	58·85/26·16	0·53(5)	4·94(8)	0·36(5)	0·03(2)	0·00(0)		98·34	10·41	
	ilm	1	0·96	19·41	1·32	58·50/12·49	0·18	2·87	0·54	0·02	0·02		96·30	33·07	
102	gl	5	63·13(96)	1·05(8)	16·18(56)	5·43(42)	0·08(6)	1·70(25)	5·59(55)	5·42(22)	0·46(1)	0·95(14)	95·39(1·21)	56·71	
	cpx	3	52·46(1·64)	1·13(11)	5·90(31)	6·04(1·21)	0·46(2)	15·37(42)	15·53(1·60)	0·77(18)	0·06(3)		97·72	51/12/37	0·289
	opx	2	54·32(52)	0·31(3)	5·14(82)	11·28(43)	0·53(12)	23·98(1·55)	4·30(1·81)	0·47(2)	0·02(2)		100·35	71/20/9	
	pl	3	54·34(35)	0·43(34)	25·19(1·08)	2·25(96)	0·02(2)	1·25(1·10)	10·70(25)	4·56(7)	0·10(1)		98·84	56·1	2·28
	mt	1	0·14	3·97	3·37	57·36/26·90	0·40	4·29	0·36	0·04	0·01		96·84	11·54	
	ilm	2	0·13	20·92	1·59	61·01/12·11	0·20	2·79	0·73	0·15	0·02		99·65	35·61	
103	gl	3	64·87(13)	0·82(23)	17·18(25)	3·92(26)	0·20(0)	2·61(10)	6·00(14)	3·87(8)	0·24(4)	0·29(0)	93·19(1·66)	74·34	
	cpx	2	48·80(45)	0·94(4)	5·83(44)	7·02(8)	0·29(0)	14·22(31)	21·49(26)	0·56(0)	0·01(1)		99·16	42/12/46	0·390
	pl	2	49·54(90)	0·15(3)	29·56(62)	2·87(7)	0·03(3)	0·47(4)	13·38(66)	3·08(32)	0·04(1)		99·12	70·4	2·80
	mt	2	0·39(21)	2·20(3)	4·56(9)	59·74/22·71	0·72(4)	6·14(5)	0·29(38)	0·03(0)	0·02(1)		96·79	5·66	
	ilm	2	0·14	14·72	1·27	69·18/8·29	0·14	2·44	0·30	0·03	0·03		96·54	23·78	
	am	4	43·16(1·43)	2·13(17)	11·95(52)	9·15(56)	0·24(6)	16·17(56)	11·70(60)	2·33(8)	0·06(2)		97·34	79·8	
104	gl	5	65·88(85)	0·84(9)	15·94(42)	4·11(16)	0·07(7)	1·81(26)	5·85(25)	4·67(26)	0·30(2)	0·52(6)	93·62(1·67)	66·45	
	cpx	3	48·70(67)	1·08(17)	5·44(3)	7·08(45)	0·39(3)	14·36(20)	20·87(32)	0·48(5)	0·02(2)		98·44	43/12/45	0·323
	opx	3	54·04(28)	0·35(13)	4·68(94)	8·79(60)	0·54(6)	28·93(2·70)	1·94(8)	0·22(15)	0·00(1)		99·50	81/15/4	
	pl	4	56·26(3·24)	0·29(47)	24·44(51)	1·85(89)	0·06(13)	1·03(9)	9·78(74)	3·11(12)	0·13(7)		96·95	62·9	2·52
	mt	2	2·38(61)	2·54(6)	4·17(1·07)	55·91/27·25	0·55(2)	5·35(5)	0·73(47)	0·01(16)	0·00(0)		98·89	7·38	
	ilm	2	0·17	17·31	1·10	63·01/10·02	0·23	2·79	0·39	0·01	0·00		95·03	28·32	

Table 4b: Continued

Run	Phase	*n*	SiO_2	TiO_2	Al_2O_3	FeO[*a]	MnO	MgO	CaO	Na_2O	K_2O	P_2O_5	Total	X_{Ph}[b]	K_d[c]
105	gl	2	65·98(1·18)	0·78(9)	16·79(6)	3·70(25)	0·13(13)	1·50(9)	5·42(10)	4·94(20)	0·34(11)	0·42(7)	93·99(75)	64·52	
	cpx	2	51·09(1·05)	1·08(15)	4·84(29)	6·94(49)	0·39(4)	14·76(56)	19·47(68)	1·36(21)	0·04(2)		99·97	45/13/42	0·274
	opx	1	56·20	0·33	3·15	11·32	0·48	26·52	2·98	0·26	0·02		101·25	75/19/6	
	pl	1	54·25	0·80	25·88	3·28	0·02	0·93	10·44	4·58	0·10		100·29	55·4	2·07
	mt	3	0·21(11)	2·74(8)	3·13(55)	59·66/26·07	0·56(11)	4·05(9)	0·38(46)	0·02(4)	0·00(0)		96·83	7·51	
	ilm	2	0·42	17·81	1·82	65·51/8·40	0·17	3·06	1·42	0·14	0·01		98·76	29·07	
106	gl	3	70·02(1·13)	0·65(9)	13·08(1·05)	3·70(2)	0·05(6)	1·21(14)	4·13(36)	5·60(92)	0·82(2)	0·75(11)	93·59(1·42)	60·48	
	cpx	2	51·00(91)	1·08(17)	6·86(36)	5·01(21)	0·43(11)	17·01(1·01)	18·20(74)	0·69(25)	0·05(2)		100·34	51/9/40	0·228
	opx	1	54·69	0·33	5·72	10·98	0·44	22·88	5·58	0·49	0·03		101·15	69/19/12	
	pl	3	55·99(89)	0·21(3)	24·77(91)	0·84(45)	0·01(0)	0·75(22)	9·85(83)	4·61(22)	0·12(5)		97·15	53·7	2·90
	mt	1	0·97	3·21	3·93	56·74/28·54	0·39	3·33	0·95	0·04	0·01		98·13	9·53	
	ilm	2	0·34	18·59	2·31	62·40/9·55	0·17	2·78	1·22	0·19	0·00		97·55	32·82	
111	gl	4	65·36(1·21)	0·91(12)	16·32(94)	4·22(65)	0·18(5)	1·73(23)	6·03(45)	4·49(64)	0·33(8)	0·43(12)	96·46(1·42)	64·74	
	cpx	2	50·32(1·04)	1·03(15)	4·70(25)	6·93(11)	0·41(6)	15·19(30)	20·91(55)	0·53(9)	0·00(1)		100·03	44/12/44	0·293
	opx	1	55·03	0·35	5·40	9·63	0·51	26·70	2·31	0·31	0·03		100·28	79/17/4	
	pl	1	55·80	0·33	24·53	2·16	0·01	2·31	11·28	3·39	0·09		99·89	64·4	2·48
	mt	2	0·87(32)	2·87(7)	4·39(25)	58·11/24·93	0·84(6)	5·22(2)	0·72(16)	0·05(3)	0·04(0)		98·05	7·62	
	ilm	2	0·86	18·62	1·14	61·92/10·61	0·35	3·25	0·69	0·02	0·02		97·48	29·03	

Notes and abbreviations are given below Table 4a.

Table 4c: Electron microprobe analyses of run products for composition B1 (QFM buffer conditions)

Run	Phase	*n*	SiO_2	TiO_2	Al_2O_3	FeO*[a]	MnO	MgO	CaO	Na_2O	K_2O	P_2O_5	Total	X_{Ph}[b]	K_d[c]
130	gl	16	50·04(18)	0·80(5)	16·03(23)	8·24(23)	0·11(6)	9·82(10)	12·62(14)	2·20(12)	0·07(2)	0·08(5)	95·71(39)	71·65	
129	gl	3	50·60(6)	0·84(0)	16·70(18)	7·84(11)	0·14(2)	8·71(7)	12·84(14)	2·22(6)	0·05(5)	0·05(5)	97·97(37)	69·23	
	ol	4	41·37(61)	0·02(2)	0·05(5)	11·28(89)	0·17(4)	47·34(95)	0·34(4)	0·02(2)	0·00(0)		100·58	88·21	0·301
128	gl	3	50·60(7)	0·87(5)	16·76(14)	7·95(14)	0·13(3)	7·74(13)	13·45(10)	2·34(12)	0·09(4)	0·09(4)	98·63(15)	65·32	
	ol	3	41·20(8)	0·03(3)	0·09(4)	11·43(17)	0·20(6)	46·93(35)	0·35(1)	0·01(1)	0·00(0)		100·23	87·98	0·257
127	gl	5	50·91(36)	0·92(8)	16·79(40)	8·04(20)	0·15(4)	7·73(12)	12·78(23)	2·47(9)	0·10(2)	0·10(2)	99·08(48)	64·09	
	ol	5	40·42(21)	0·02(2)	0·12(9)	13·79(25)	0·22(6)	45·92(27)	0·32(4)	0·02(2)	0·00(0)		100·83	85·58	0·295
	cpx	5	51·50(1·36)	0·51(5)	4·90(88)	6·33(33)	0·14(5)	16·31(74)	20·63(53)	0·33(13)	0·01(1)		100·67	47/10/43	0·296
	pl	2	50·09(51)	0·11(2)	30·07(22)	1·19(6)	0·00(0)	0·75(5)	15·74(50)	2·65(14)	0·02(1)		100·62	76·6	1·15
134	gl	6	50·32(25)	0·80(3)	16·90(12)	8·07(24)	0·19(7)	8·11(14)	13·23(18)	2·15(9)	0·09(3)	0·13(9)	94·69(79)	68·39	
	ol	3	39·92(9)	0·04(2)	0·05(7)	13·48(1·01)	0·21(2)	45·40(95)	0·37(5)	0·01(2)	0·01(1)		99·51	85·72	0·360
132	gl	5	50·75(40)	0·87(2)	17·62(33)	8·62(42)	0·17(5)	6·78(17)	12·60(18)	2·38(10)	0·08(2)	0·11(8)	97·59(22)	61·41	
	ol	4	39·78(17)	0·04(1)	0·08(3)	14·73(66)	0·26(10)	43·25(76)	0·34(4)	0·03(2)	0·00(0)		98·52	83·69	0·304
	cpx	5	51·27(85)	0·49(2)	4·85(62)	6·36(79)	0·18(7)	14·99(41)	20·80(72)	0·22(3)	0·01(1)		99·16	45/11/44	0·379
	pl	5	47·14(43)	0·05(5)	32·42(31)	0·95(8)	0·01(2)	0·44(11)	17·48(16)	1·64(8)	0·03(1)		100·16	85·4	2·02
133	gl	9	51·70(68)	1·04(9)	16·53(82)	8·77(31)	0·12(4)	7·30(67)	11·72(61)	2·68(22)	0·08(3)	0·07(6)	98·15(68)	62·14	
	ol	9	40·14(30)	0·02(1)	0·11(5)	16·81(86)	0·25(9)	43·10(63)	0·35(4)	0·02(2)	0·01(1)		100·81	82·05	0·359
	cpx	4	52·47(81)	0·59(10)	4·88(1·36)	6·94(68)	0·16(2)	15·60(90)	20·49(1·13)	0·31(9)	0·01(2)		101·45	45/12/43	0·410
	pl	4	49·78(57)	0·12(6)	30·29(1·33)	1·31(33)	0·02(2)	1·22(69)	16·18(17)	2·13(19)	0·03(1)		101·08	80·6	1·73
131	gl	6	51·26(27)	1·19(14)	17·52(1·25)	9·20(59)	0·19(10)	5·63(33)	12·04(29)	2·70(19)	0·11(2)	0·16(4)	98·89(75)	53·87	
	ol	5	39·01(10)	0·03(1)	0·18(18)	19·71(63)	0·29(7)	39·47(64)	0·33(8)	0·02(2)	0·01(1)		99·06	78·11	0·327
	cpx	3	50·54(66)	0·67(8)	4·86(46)	8·42(46)	0·24(3)	15·22(38)	19·18(42)	0·33(3)	0·02(1)		99·47	45/14/41	0·322
	pl	6	51·15(1·04)	0·18(10)	28·44(1·70)	1·32(50)	0·04(2)	0·95(62)	14·56(63)	3·04(38)	0·04(2)		99·70	72·4	1·07
142	gl	13	50·54(66)	0·90(5)	18·78(25)	8·54(43)	0·11(6)	5·94(18)	12·30(35)	2·73(41)	0·08(5)	0·10(6)	93·48(79)	59·77	
	ol	8	39·63(33)	0·03(2)	0·05(2)	17·33(58)	0·24(6)	42·11(77)	0·36(4)	0·01(1)	0·01(1)		99·77	81·25	0·343
	cpx	7	50·97(1·00)	0·65(12)	6·02(1·65)	6·48(66)	0·12(3)	15·00(1·58)	20·39(82)	0·28(15)	0·02(1)		99·93	45/11/44	0·360
141	gl	11	51·34(76)	1·07(10)	17·95(93)	9·45(45)	0·17(7)	5·93(58)	10·84(67)	2·98(26)	0·10(4)	0·16(6)	96·44(36)	56·50	
	ol	8	39·47(36)	0·02(2)	0·06(6)	19·78(56)	0·32(5)	39·43(1·30)	0·32(5)	0·09(23)	0·01(1)		99·50	78·04	0·365
	cpx	3	49·67(1·86)	0·75(15)	5·50(1·43)	7·77(79)	0·18(7)	15·12(79)	21·05(77)	0·21(6)	0·01(1)		100·27	44/12/44	0·238
	pl	3	47·58(88)	0·07(3)	32·54(47)	0·97(24)	0·04(4)	0·41(10)	17·14(43)	1·73(24)	0·03(1)		100·51	84·4	2·72
140	gl	4	53·06(49)	1·58(2)	18·05(59)	9·66(60)	0·14(11)	3·95(66)	9·79(34)	3·49(48)	0·19(6)	0·11(5)	96·73(2·21)	45·62	
	ol	4	38·43(14)	0·04(2)	0·08(3)	23·51(28)	0·34(9)	38·16(17)	0·37(3)	0·02(4)	0·00(0)		100·94	74·56	0·290
	cpx	5	50·55(91)	0·74(6)	4·81(91)	8·41(99)	0·19(3)	15·46(33)	19·82(73)	0·29(21)	0·01(1)		100·29	45/14/41	0·201
	pl	6	50·10(56)	0·33(13)	27·78(2·71)	2·38(78)	0·04(4)	1·56(77)	14·54(10)	2·65(34)	0·04(2)		99·42	75·1	1·96

Table 4c: Continued

Run	Phase	*n*	SiO_2	TiO_2	Al_2O_3	FeO*[a]	MnO	MgO	CaO	Na_2O	K_2O	P_2O_5	Total	X_{Ph}[b]	K_d[c]
143	gl	7	53·07(57)	2·01(23)	17·65(1·12)	10·95(87)	0·23(4)	4·06(33)	9·34(56)	2·23(27)	0·22(3)	0·25(6)	97·82(1·35)	42·40	
	ol	4	37·86(21)	0·05(2)	0·10(8)	24·90(1·02)	0·39(4)	36·51(52)	0·43(2)	0·03(3)	0·01(1)		100·27	72·55	0·282
	cpx	4	50·37(60)	0·84(2)	4·95(1·01)	8·94(76)	0·23(7)	14·91(85)	19·39(62)	0·34(8)	0·01(1)		99·97	44/15/41	0·215
	pl	5	50·95(43)	0·14(7)	29·69(86)	1·10(15)	0·02(3)	0·49(16)	14·37(31)	3·04(29)	0·03(2)		99·83	72·2	1·13
148	gl	7	53·26(62)	1·25(4)	19·25(32)	8·55(30)	0·17(10)	3·78(24)	9·54(26)	3·93(34)	0·16(4)	0·12(6)	92·99(1·46)	48·67	
	ol	4	38·26(31)	0·03(1)	0·02(1)	23·60(58)	0·36(4)	38·51(22)	0·35(5)	0·02(2)	0·02(1)		101·16	75·31	0·326
	cpx	3	48·90(1·36)	1·17(42)	6·52(1·82)	7·10(72)	0·13(4)	14·26(1·07)	21·78(73)	0·21(8)	0·00(0)		100·08	42/12/46	0·190
	pl	4	48·20(38)	0·03(2)	32·97(47)	0·70(14)	0·03(3)	0·15(19)	16·17(40)	2·30(21)	0·02(1)		100·57	79·4	2·89
147	gl	6	53·50(29)	1·49(3)	18·94(23)	8·89(41)	0·24(16)	3·80(41)	8·75(14)	4·05(25)	0·17(2)	0·16(8)	93·23(83)	47·77	
	ol	6	37·88(25)	0·04(2)	0·06(3)	25·40(38)	0·40(3)	37·16(33)	0·38(4)	0·09(5)	0·00(0)		101·41	73·52	0·351
	cpx	4	50·43(39)	0·89(7)	4·75(31)	8·25(62)	0·25(4)	14·92(54)	20·21(92)	0·25(18)	0·01(1)		99·97	44/14/42	0·246
	pl	2	48·57(22)	0·14(7)	31·82(70)	0·99(15)	0·03(4)	0·46(4)	15·82(36)	2·32(1)	0·03(1)		100·18	78·9	3·15
146	gl	3	53·77(1·65)	1·80(17)	18·56(1·33)	9·40(32)	0·14(10)	3·23(33)	8·27(63)	4·55(21)	0·17(3)	0·11(11)	94·69(1·97)	42·42	
	ol	5	37·52(54)	0·05(1)	0·29(26)	26·61(61)	0·41(5)	35·64(93)	0·47(15)	0·00(0)	0·00(1)		101·00	71·08	0·308
	cpx	10	49·73(79)	1·23(13)	6·49(1·40)	9·07(60)	0·20(5)	13·60(22)	18·02(60)	0·22(21)	0·02(2)		98·59	43/16/41	0·276
	pl	3	50·88(1·15)	0·41(23)	27·37(1·55)	2·25(94)	0·06(4)	1·39(60)	13·25(86)	2·77(53)	0·04(2)		98·43	72·4	2·63
145	gl	6	56·14(68)	1·90(10)	17·23(65)	9·30(46)	0·12(11)	2·91(35)	7·39(35)	4·67(26)	0·17(3)	0·17(8)	95·57(1·05)	39·49	
	ol	10	38·18(47)	0·06(2)	0·27(31)	25·73(82)	0·41(4)	34·58(76)	0·43(13)	0·03(5)	0·00(0)		99·70	70·56	0·272
	cpx	6	51·01(86)	1·17(15)	5·67(1·89)	8·48(40)	0·20(5)	13·44(1·23)	18·88(1·20)	0·40(10)	0·03(2)		99·27	42/15/43	0·231
	pl	5	50·41(51)	0·25(8)	28·53(1·06)	1·73(31)	0·04(04)	1·09(57)	13·61(60)	3·09(25)	0·03(1)		98·78	70·8	2·79
153	gl	3	58·46(33)	1·18(3)	17·59(16)	8·97(12)	0·09(4)	2·52(48)	6·60(12)	4·15(54)	0·23(3)	0·21(14)	92·75(10)	37·62	
	ol	3	37·19(3)	0·01(1)	0·04(0)	30·33(30)	0·39(2)	32·56(12)	0·26(3)	0·00(1)	0·01(2)		100·79	65·77	0·315
	cpx	3	51·10(29)	0·62(6)	3·60(49)	10·60(52)	0·29(8)	15·49(15)	17·84(67)	0·13(11)	0·02(1)		99·68	45/18/37	0·224
	pl	3	49·21(33)	0·14(3)	30·84(64)	1·40(8)	0·06(4)	0·33(30)	15·07(26)	2·52(5)	0·03(2)		99·59	76·6	3·76
	am	3	43·02(51)	1·97(45)	13·24(73)	11·62(13)	0·16(5)	14·51(43)	10·64(22)	2·52(18)	0·07(3)		97·74	74·4	
152	gl	2	60·06(44)	1·13(36)	16·77(49)	8·93(1·35)	0·11(8)	2·31(66)	5·81(33)	4·36(74)	0·27(3)	0·25(11)	93·56(1·89)	35·71	
	ol	3	36·80(10)	0·05(1)	0·10(8)	30·73(46)	0·45(5)	32·14(65)	0·32(11)	0·00(1)	0·01(2)		100·60	65·56	0·298
	cpx	3	51·59(19)	0·70(3)	3·37(6)	10·03(51)	0·31(6)	15·17(16)	19·10(62)	0·19(12)	0·01(1)		100·47	44/16/40	0·197
	pl	4	50·37(58)	0·12(5)	29·68(1·02)	1·36(37)	0·02(2)	1·01(66)	14·24(49)	2·96(27)	0·03(1)		99·80	72·5	3·61
	am	6	43·08(98)	2·82(1·01)	12·08(17)	11·83(34)	0·14(4)	14·63(22)	11·37(38)	2·37(41)	0·07(1)		98·40	72·9	
151	gl	2	61·33(88)	1·17(16)	17·98(1·71)	7·49(98)	0·10(5)	1·84(27)	4·98(90)	4·67(70)	0·18(2)	0·26(9)	92·89(2·64)	34·53	
	ol	3	37·19(38)	0·06(2)	0·34(6)	30·44(29)	0·40(8)	32·57(91)	0·27(18)	0·01(1)	0·01(1)		101·28	65·77	0·276
	cpx	3	50·38(73)	1·02(11)	5·27(98)	10·38(68)	0·21(1)	14·90(25)	18·07(1·09)	0·48(8)	0·02(0)		100·73	44/18/38	0·178
	pl	2	51·82(8)	0·15(9)	29·37(1·19)	1·34(46)	0·06(6)	0·51(45)	13·19(22)	3·79(25)	0·04(1)		100·28	65·5	3·26
	am	6	43·12(31)	2·73(63)	12·44(99)	12·11(27)	0·14(4)	14·21(16)	11·14(46)	2·57(27)	0·09(1)		98·55	85·2	
	ilm	3	3·94(1·67)	46·61(1·79)	1·65(1·25)	5·23/34·28	0·43(3)	5·78(17)	1·04(48)	0·06(3)	0·01(0)		99·04	71·6	

Notes and abbreviations are given below Table 4a.

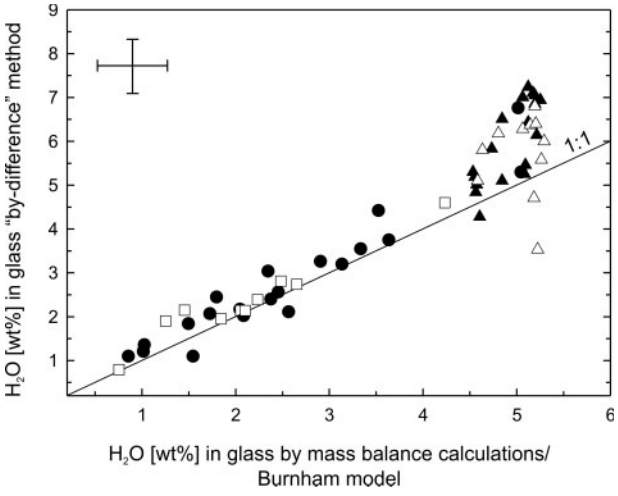

Fig. 2. Comparison of melt water contents for B1 and B2 calculated by mass balance ($a_{H_2O} < 1$; ●, B1; □, B2) and by using the 'Burnham model' ($a_{H_2O} = 1$; ▲, B1; △, B2) with the H_2O contents obtained with the 'by-difference' method (Devine *et al.*, 1995; Koepke, 1997). Error bars correspond to the average errors obtained for values using the 'by-difference' method (±1·23 wt %) and mass balance calculations (±0·74 wt %) assuming an error of 20% relative for phases with 1–10 wt % abundances.

and stability of experimental phases. For example, in B1 experiments at 1000°C, orthopyroxene is stable only at low bulk water contents (0·89 and 1·49 wt % H_2O) and the stability of amphibole is reached only at the highest bulk water content of 4·70 wt % (Fig. 4a).

A further point is that a change in the water content of the melt (and thus a_{H_2O}), while holding all other parameters constant, results in a change of f_{O_2} (see above). Oxygen fugacity is identical in all runs with $a_{H_2O} = 1$ at isothermal conditions. In this case the f_{O_2} corresponds to the adjusted f_{O_2} conditions of the IHPV. In contrast, at higher temperatures, when H_2O saturation has not been reached, f_{O_2} depends also on the prevailing a_{H_2O} (Scaillet *et al.*, 1995; Table 3). Hence, it is difficult to discriminate between the individual effects of a_{H_2O} and f_{O_2}, especially in the discussion on the evolution of iron-bearing phases.

Achievement of equilibrium

Crystallization experiments are known to be the best method to approach equilibrium conditions (Pichavant, 1987) when compared with melting experiments in which non-equilibrated residual minerals can remain for long run durations in the surrounding melt. The following observations are taken as evidence for near-equilibrium conditions. (1) All phases are typically homogeneous and their compositions change with the experimental conditions, following systematic compositional trends. (2) The crystal distribution is homogeneous in all experiments (Fig. 3a–c). (3) Phase relations and compositions were identical in runs performed at identical conditions and for different run duration (24 h and up to 96 h), at high and at low temperatures (for B1 compare runs 62 and 61 with 45 and 42, respectively, and for B2 compare run 111 with 104; Table 3a and b). (4) Mineral–melt and mineral–mineral partitioning coefficients (for olivine, plagioclase, amphibole and Fe–Ti oxides) are in good agreement with published data from other studies (see below). (5) The formation of quench crystals was avoided (Fig. 3a–c) so that there is no need to distinguish between quench and stable phases or to perform integrative measurements of glass and quench crystals, as has been done in previous studies (e.g. Helz, 1976).

RESULTS

Phase relations

Experimental results and phase proportions are listed in Table 3. Phase relations for compositions B1 and B2 are shown in T–H_2O diagrams (Fig. 4). The influence of water on phase relations is presented in terms of both bulk water content and contours of equal a_{H_2O} in the melt. The relation between a_{H_2O} and water content of the melt is given in Table 3.

Primitive MORB system (B1) at MnO–Mn_3O_4 buffer conditions

Olivine is the liquidus phase for all bulk water contents (Fig. 4a). At $a_{H_2O} = 1$ and $a_{H_2O} = 0·6$ the saturation boundary is at about 1125°C and 1150°C, respectively. In runs below 1000°C olivine is no longer stable. This is in agreement with the decreasing calculated modal abundance of olivine at 1000°C compared with 1050°C (Table 3a) and with changes from euhedral to rounded olivine crystals at 1050°C and 1000°C. Plagioclase and clinopyroxene saturation curves are almost identical and the relative order of crystallization is unknown. Plagioclase and clinopyroxene start to crystallize between 1100°C and 1050°C at $a_{H_2O} = 1$ and at about 1150°C at $a_{H_2O} = 0·2$. Magnetite was found below 1050°C. Amphibole is stable under nearly water-saturated conditions only. It is present in all runs at 950°C and at 1000°C with 4·70 wt % bulk H_2O content. Orthopyroxene is stable in runs with 0·89 and 1·49 wt % bulk H_2O content at 1000°C and in all runs at 950°C. The ilmenite stability field is restricted to 950°C in charges with 0·89 and 1·49 wt % bulk H_2O content.

Differentiated MORB system (B2) at MnO–Mn_3O_4 buffer conditions

In contrast to B1, olivine was not observed in experiments using the B2 starting composition. Magnetite crystallizes as the liquidus phase for all bulk water contents (Fig. 4b) and its liquidus temperature is below 1150°C for a bulk water content of 4·50 wt %. Clinopyroxene is observed

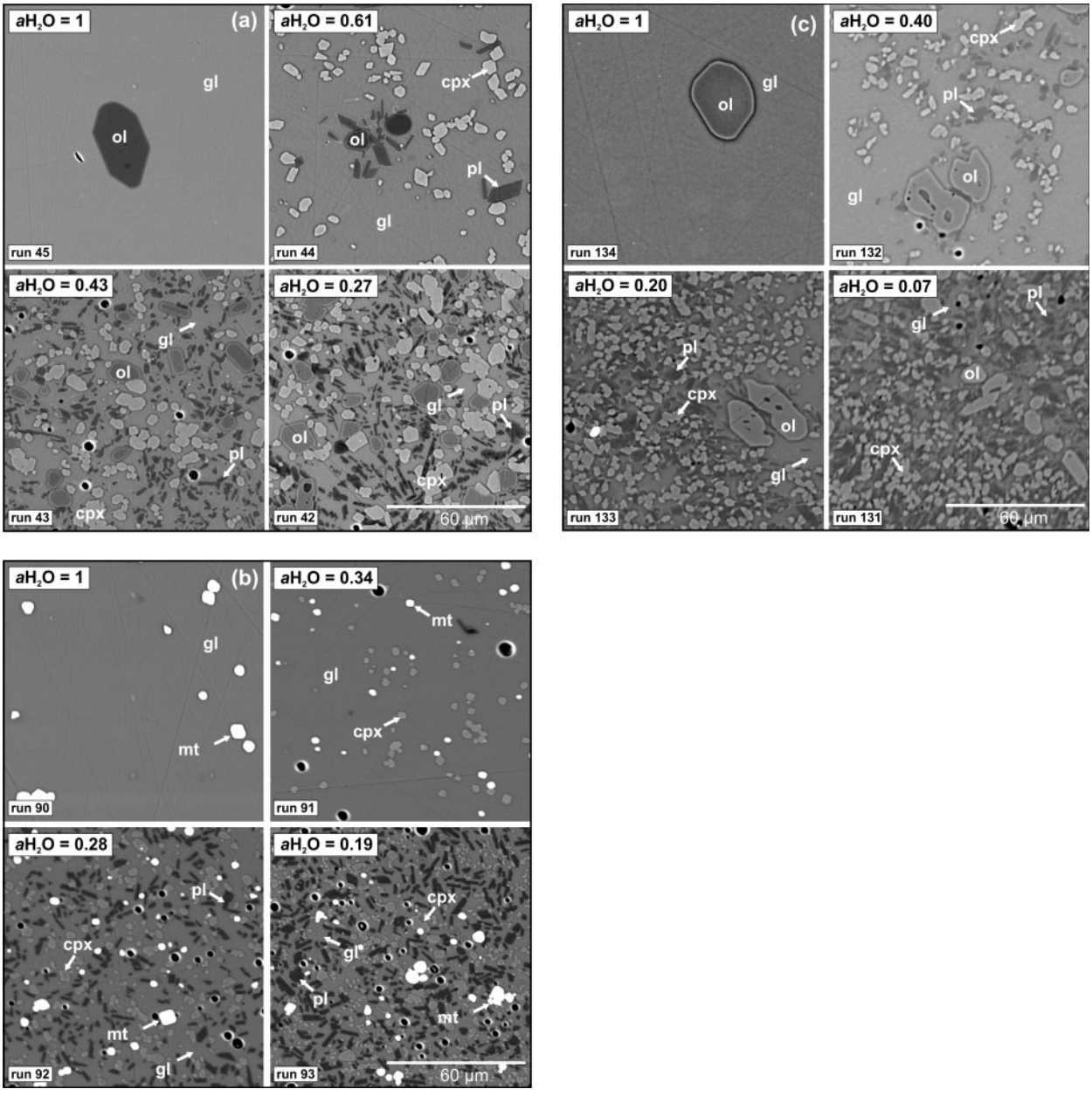

Fig. 3. Back-scattered electron (BSE) images of run products obtained at 1100°C at MnO–Mn_3O_4 buffer conditions (a, B1; b, B2) and QFM buffer conditions (c, B1). gl, glass; ol, olivine; pl, plagioclase; cpx, clinopyroxene; mt, magnetite. Images show variation in modal proportion and phase stability in experiments with varying bulk water content and thus a_{H_2O} of the charge for a constant temperature. The absence of quench crystals should be noted.

between 1100°C and 1050°C at $a_{H_2O} = 1$ and 1150°C and 1100°C for $a_{H_2O} < 0{\cdot}3$. The plagioclase saturation curve depends strongly on a_{H_2O}. At water-saturated conditions plagioclase is stable only below 1000°C. At lower water activities the saturation temperature of plagioclase rises to 1100°C ($a_{H_2O} = 0{\cdot}25$). The ilmenite saturation curve depends also on a_{H_2O} and is approximately 50°C below that of plagioclase. In contrast to B1, orthopyroxene is observed in B2 at higher temperature for low bulk water contents. It crystallizes at 1050°C for an a_{H_2O} of 0·38 (run 96; Table 3b) but is not stable at 950°C and 4·5 wt % bulk H_2O.

Primitive MORB system (B1) at QFM buffer conditions

Olivine is the liquidus phase for all bulk water contents and starts to crystallize between 1125°C and 1150°C at

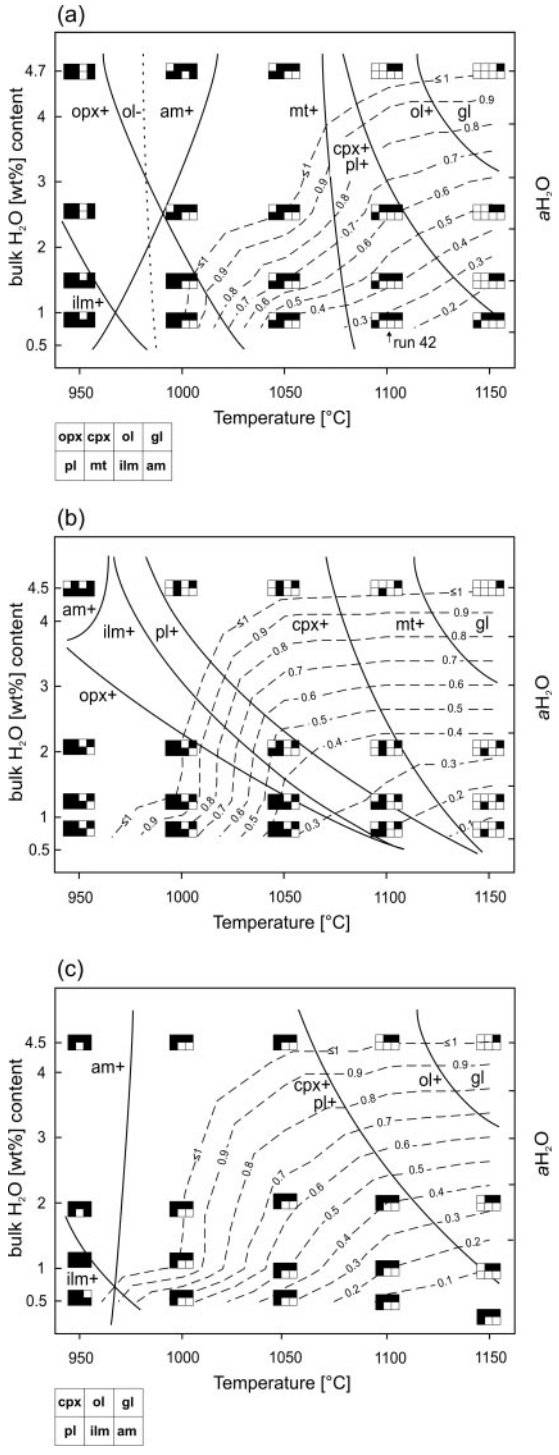

Fig. 4. Phase relations of B1 (a) and B2 (b) compositions at MnO–Mn_3O_4 buffer conditions and B1 (c) at QFM buffer conditions as a function of temperature and bulk water content contoured for a_{H_2O} (dashed lines) at 200 MPa. gl, glass; ol, olivine; pl, plagioclase; cpx, clinopyroxene; mt, magnetite; ilm, ilmenite; am, amphibole. Continuous lines indicate beginning of crystallization of a phase. Dotted lines mark phase-out boundary. Contours of a_{H_2O} are based on a_{H_2O} calculated after Burnham (1979; Tables 2 and 3) and extrapolated between different runs.

water-saturated conditions (Table 3c; Fig. 4c). At $a_{H_2O} <$ 0·4 olivine crystallizes at temperatures higher than 1150°C. The plagioclase and clinopyroxene saturation temperature is about 50°C below that of olivine. Amphibole is stable only in experiments at 950°C in which water-saturated conditions have been reached even for low bulk water contents. Ilmenite crystallizes in runs 151 and 150 at 950°C (1·12 and 0·55 wt % bulk water content, respectively).

The solidus temperature was reached in run 150 and crystals were too small to be analysed correctly. Thus, ilmenite as well as all other phases were identified only qualitatively in this experiment by back-scattered electron images.

At a given temperature, the phase diagrams at both low and high f_{O_2} (Fig. 4) show variations in the phase assemblages within the fluid-saturated field. This is attributed to the effect of the dilution of the fluid phase by air (see discussion above), resulting in a slight decrease of a_{H_2O} in capsules with low bulk water content (higher N_2/Ar ratio).

Phase chemistry

Olivine

X_{Fo} of olivines obtained at MnO–Mn_3O_4 buffer conditions are generally higher (X_{Fo} between 92 and 83; Fig. 5a) than at QFM buffer conditions (X_{Fo} between 88 and 66; Fig. 5b). At constant temperature, X_{Fo} varies as a function of bulk water content (e.g. at 1100°C from X_{Fo92} to X_{Fo84} for a bulk water content of 4·7 and 0·89, respectively; Fig. 5a). At high f_{O_2} X_{Fo} falls with falling temperature from 1150 to 1050°C to minimum values of X_{Fo89} (4·70 wt % bulk H_2O content) and X_{Fo83} (0·89 wt % bulk H_2O content), but rises again at temperatures <1050°C. This is a consequence of increasing magnetite crystallization leading to slightly higher MgO and lower FeO* (total iron) concentrations in the melt (Figs 5 and 9; Table 4a). At low f_{O_2}, the minimum X_{Fo} is observed in olivine crystallizing at 950°C and is identical, independent of bulk water content (X_{Fo} of 66). This is related to melt Mg-number, which is almost identical in all 950°C experiments (ranging from 38 to 35 for all bulk water contents).

One of the most significant minor elements in olivine is calcium (Libourel, 1999), with concentrations depending on X_{Fo} ranging between 0·19 wt % and 0·47 wt % CaO (Table 4a and c). It is generally accepted that neither oxygen fugacity, nor temperature or pressure, directly influence Ca partitioning (Roeder, 1974; Longhi *et al.*, 1978; Watson, 1979; Jurewicz & Watson, 1988; Libourel, 1999). As demonstrated by Libourel (1999), Ca concentration in olivine depends on the olivine composition as well as on the alkali and alumina content of the melt. Generally, the partition coefficient $D_{CaO}^{Ol-Melt}$

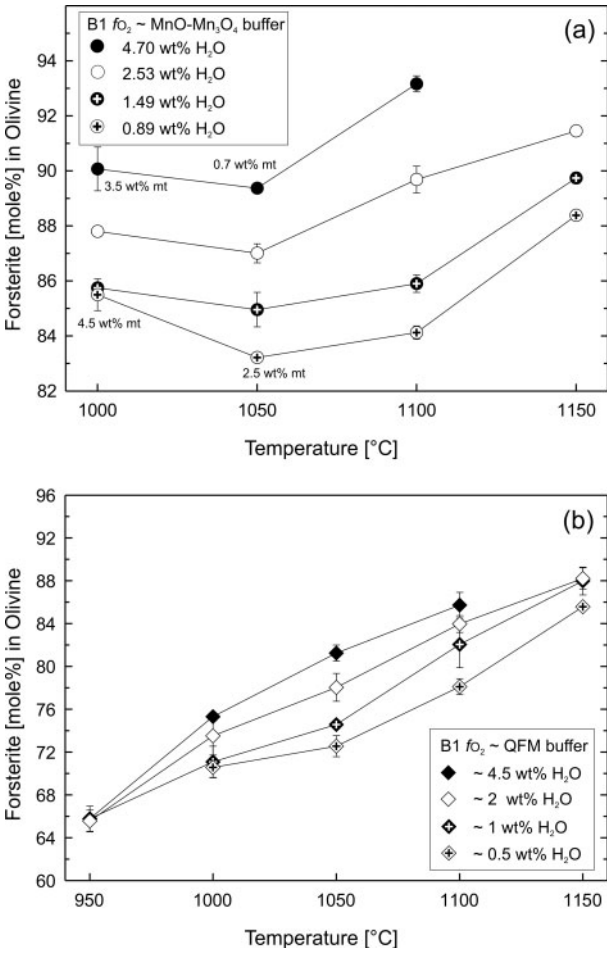

Fig. 5. Olivine composition in B1 as a function of temperature and bulk water content at MnO–Mn_3O_4 buffer conditions (a) and QFM (b). Error bars correspond to the standard deviation of average olivine compositions. For bulk water contents of 4·70 and 0·89 wt % numbers indicate the proportion of magnetite (wt % mt).

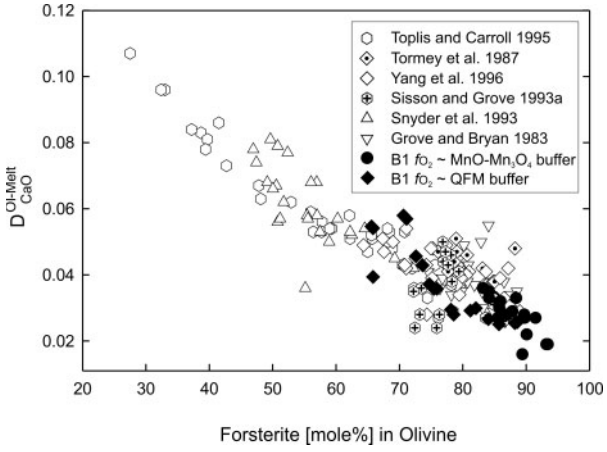

Fig. 6. $D^{Ol-Melt}_{CaO}$ vs the forsterite content of olivine. Additional data for various natural basaltic compositions from other studies as in Fig. 12. Error for $D^{Ol-Melt}_{CaO}$ is typically ±0·004 and has been obtained by error propagation calculating $D^{Ol-Melt}_{CaO}$ from the standard deviation of CaO concentrations in olivine and melt. Errors in olivine compositions are given in Fig. 5.

($CaO_{Olivine}/CaO_{Melt}$, in wt %) increases with decreasing X_{Fo} and increasing melt alkali and CaO content. Figure 6 shows $D^{Ol-Melt}_{CaO}$ vs X_{Fo} obtained in this study. As expected from the generally high X_{Fo} and low melt alkali content, Ca concentration in olivine is typically low in our system. Comparison with other data from experimental studies on more iron-rich, tholeiitic and other basaltic systems confirms $D^{Ol-Melt}_{CaO}$ values obtained in this study, suggesting equilibrium conditions with respect to Ca partitioning between olivine and melt.

Pyroxene

Clinopyroxene and orthopyroxene obtained in runs with B1 at high f_{O_2} vary only moderately with changing experimental conditions and have an average composition of $En_{45}Fs_{12}Wo_{43}$ (± 1·3 mol %) and $En_{82}Fs_1Wo_3$ (± 0·9 mol %), respectively (Table 4a). Clinopyroxene synthesized in experiments with composition B2 is characterized by a larger compositional variation (Table 4b). At water-saturated conditions clinopyroxene has an average composition of $En_{42}Fs_{12}Wo_{46}$ (±2·3 mol %; 4·50 wt % bulk water content), which changes continuously with decreasing bulk water content to $En_{48}Fs_{13}Wo_{39}$ (±1·4 mol %; 0·74 wt % bulk water content). B2 orthopyroxene in equilibrium with the most En-rich clinopyroxene crystallized at 0·74 wt % bulk water content has the highest Wo content ($En_{71}Fs_{20}Wo_9$ ± 2·2 mol %). All other orthopyroxenes vary only little in their mole proportions ($En_{79}Fs_{16}Wo_5$ ± 2 mol %), showing slight decreases in Fs and Wo contents with increasing bulk water content. At QFM buffer conditions clinopyroxene has an average composition of $En_{44}Fs_{14}Wo_{42}$ ± 2 mol %. The average $K^{Cpx-Melt}_{D_{Fe-Mg}}$ of clinopyroxene [defined as $(X_{Cpx-FeO}/X_{Cpx-MgO}) \times (X_{Melt-MgO}/X_{Melt-FeO})$] is 0·26 but generally increases with melt Mg-number. As reported by Hoover & Irvine (1977) and Toplis & Carroll (1995), $K^{Cpx-Melt}_{D_{Fe-Mg}}$ values increase independently of f_{O_2} with increasing melt Mg-number up to 0·26 (for melt Mg-number of about 40). At QFM buffer conditions for relatively low melt Mg-number, the obtained $K^{Cpx-Melt}_{D_{Fe-Mg}}$ values are in good agreement with published data (Table 4). For melt Mg-number above 50, the $K^{Cpx-Melt}_{D_{Fe-Mg}}$ deviates from the linear trend with values up to 0·41. The same observation has been made for partitioning of Mg and Fe^{2+} between clinopyroxene and melt under MnO–Mn_3O_4 buffer conditions, which confirms that there is no dependence of $K^{Cpx-Melt}_{D_{Fe-Mg}}$ on f_{O_2} (Toplis & Carroll, 1995). It is noteworthy that the bulk water content has no influence on $K^{Cpx-Melt}_{D_{Fe-Mg}}$.

Plagioclase

The composition of plagioclase as a function of temperature and H_2O is shown in Fig. 7. The anorthite (An) content decreases continuously by ~0·05 mol % per °C with falling temperature for all bulk water contents. Plagioclase synthesized at high f_{O_2} is slightly more An-rich than that crystallized at similar T–H_2O conditions and low f_{O_2}. Consequently, the highest An contents (An_{88}, 1050°C; An_{79}, 950°C) are obtained for B1 in runs with 4·70 wt % bulk H_2O content (Fig. 7a). The most Ab-rich plagioclase for B1 (An_{66}; Fig. 7b) is stable at 950°C with 1·12 wt % bulk water content. In agreement with previous studies (e.g. Turner & Verhoogen, 1960; Carmichael *et al.*, 1974; Panjasawatwong *et al.*, 1995; Martel *et al.*, 1998; Scaillet & Evans, 1999; Berndt *et al.*, 2001), at a given temperature the An content of plagioclase increases with increasing melt water content and therefore increasing a_{H_2O}. However, at fluid-saturated conditions, the plagioclase compositions are also systematically more Ca rich with increasing bulk water content, although the same melt water content ($a_{H_2O} = 1$) apparently has been reached in runs at lower temperatures. This is attributed to the presence of N_2 in the capsules (as already discussed), resulting in a slight decrease of water activity with decreasing bulk water content and higher N_2/H_2O ratio.

The direct influence of H_2O on plagioclase–liquid equilibrium compositions is shown in Fig. 8. For a constant Ca/Na ratio in the melt, the An content of plagioclase obtained at nearly water-saturated conditions (4·55–5·25 wt % H_2O in melt) is noticeably higher when compared with An contents in plagioclases in equilibrium with melts containing about 2 wt % H_2O. Consequently, $K_{D_{Ca-Na}}^{Pl-Melt}$ [defined as molar $(Ca/Na)_{Plag}/(Ca/Na)_{Liq}$] increases with increasing a_{H_2O} of the melt. Continuous lines in Fig. 8 indicate $K_{D_{Ca-Na}}^{Pl-Melt}$ values given by Sisson & Grove (1993*a*) for plagioclase–melt pairs obtained in high-alumina basalts with 4 wt % H_2O in the melt at 100 MPa ($K_{D_{Ca-Na}}^{Pl-Melt} \sim 3{\cdot}4$; Sisson & Grove, 1993*b*) and 2 wt % H_2O in the melt at 200 and 500 MPa ($K_{D_{Ca-Na}}^{Pl-Melt} \sim 1{\cdot}7$; Baker & Eggler, 1987). This indicates that the effect of pressure variations between 100 and 500 MPa on $K_{D_{Ca-Na}}^{Pl-Melt}$ is negligible. As emphasized by Sisson & Grove (1993*a*,) the pressure dependence of $K_{D_{Ca-Na}}^{Pl-Melt}$ in dry systems in the range 1 atm to 20 kbar is always significantly lower than the influence of water. $K_{D_{Ca-Na}}^{Pl-Melt}$ values obtained in this study for given melt water contents in primitive and differentiated MORB compositions agree well with the data of Sisson & Grove (1993*a*, 1993*b*) and Baker & Eggler (1987) for high-alumina basalts. This confirms that plagioclase composition mainly depends on a_{H_2O} and melt Ca/Na.

Compared with experimental studies in dry systems (e.g. Toplis & Carroll, 1995), the An content of plagioclase obtained in our study decreases only by about 0·05 mol % per °C [compared with 0·5 mol % per °C in

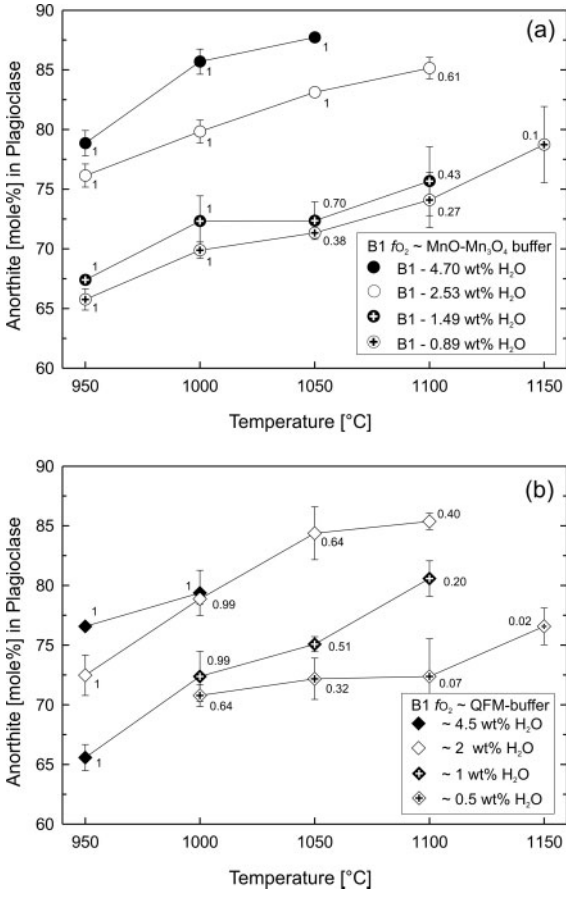

Fig. 7. Plagioclase composition in B1 as a function of temperature and bulk water content at MnO–Mn_3O_4 buffer conditions (a) and QFM (b). Errors bars correspond to the standard deviation of average plagioclase compositions. Water contents are given as bulk water contents. Numbers indicate a_{H_2O} of the melt.

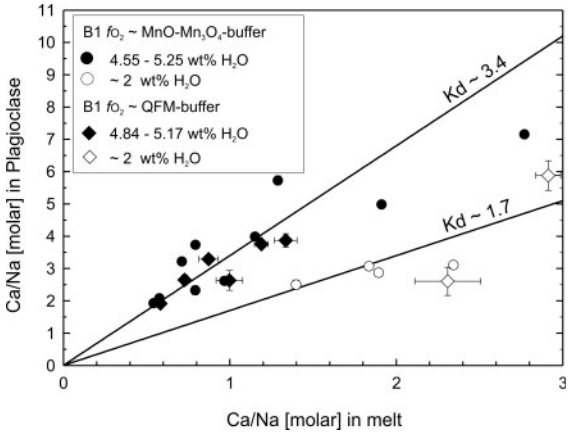

Fig. 8. Ca/Na ratios for plagioclase–melt pairs in B1 obtained at water-saturated conditions [$a_{H_2O} = 1$; melt water contents calculated after Burnham (1979); Table 3] and *c.* 2 wt % H_2O in the melt. Continuous lines show $K_{D_{Ca-Na}}^{Pl-Melt}$, after Sisson & Grove (1993*a*) for plagioclase–melt pairs in high-alumina basalt (Sisson & Grove, 1993*b*) at 100 MPa and about 4 wt % H_2O in melt ($K_{D_{Ca-Na}}^{Pl-Melt} \sim 3{\cdot}4$), and about 2 wt % H_2O in melt at 200 and 500 MPa (Baker & Eggler, 1987; $K_D \sim 1{\cdot}7$).

the study of Toplis & Carroll (1995) for a given bulk water content with falling temperature (Fig. 7)]. As discussed above, in water-bearing systems, for a given bulk water content, increasing crystal fraction (as a result of falling temperature) results in an increase of melt water content. Thus, the effect of decreasing Ca/Na in the melt with progressive crystallization, resulting in a strong decrease of An content in dry systems, is compensated by increasing melt water content.

Amphibole

According to the classification of Leake *et al.* (1997) the synthesized amphibole is pargasite. The Mg-number of amphibole (calculated with all iron as FeO*) increases with increasing bulk water content (Table 4). The number of Si atoms in the tetrahedral position of the amphibole synthesized at 1000°C is lower than that of amphibole obtained at 950°C, whereas Al^{IV} increases with rising temperature. This is in agreement with previous experimental studies (Helz, 1981; Sisson & Grove, 1993*a*). At 950°C, Si and Al remain constant for all bulk water contents. Sisson & Grove (1993*a*) showed that the tetrahedral Al/Si ratio of amphibole is linearly related to the Al/Si ratio of the melt and can be described as $K_{D_{Al-Si}}^{Am-Melt} = (X_{Al}/X_{Si})_{Am}/(X_{Al}/X_{Si})_{Melt}$. An average $K_{D_{Al-Si}}^{Am-Melt}$ of 1·01 (±0·08) from coexisting liquid–amphibole pairs obtained in B1 and B2 agrees well with the value of 0·94 (±0·06) given by Sisson & Grove (1993*a*) for liquid–amphibole couples in compositions ranging from high-alumina basalt to high-silica rhyolite.

The occurrence of amphibole in natural systems is often used to argue whether magmas were 'dry' or hydrous in a broadly qualitative sense. Our results support previous experimental findings in hydrous basaltic and calc-alkaline systems (e.g. Holloway & Burnham, 1972; Helz, 1973; Spulber & Rutherford, 1983; Sisson & Grove, 1993*a*; Johnson *et al.*, 1994) showing that a relatively high amount of H_2O in the melt is necessary to stabilize amphibole (~5 wt % in our study). In our study the stability field of amphibole is always restricted to runs under nearly water-saturated conditions (Fig. 4); however, not all experiments containing a free fluid phase contain amphibole, probably because of higher N_2/H_2O ratio in charges with low bulk water contents and thus slightly lower a_{H_2O} (see above). This indicates that very small variations in a_{H_2O} may influence amphibole stability. However, the absence of amphibole is clearly not evidence for 'dry' conditions.

Fe–Ti oxides

Owing to the small size of magnetite and ilmenite crystals, analyses of these phases are often contaminated by the surrounding glass as indicated by variable SiO_2 contents (Table 4a and b). However, no attempt was made to correct the analyses.

Magnetite in B1 and B2, which is stable only at high f_{O_2}, is characterized by relatively low ulvöspinel contents [X_{Usp}; calculated after Andersen *et al.* (1993)] ranging from 5 to 19 mol %, depending mainly on the bulk water content and, to a lesser extent, on temperature. X_{Usp} systematically increases with decreasing bulk water content for all temperatures (Table 4a and b).

For a given temperature, X_{Usp} in B1 experiments with different bulk water contents remains relatively constant (e.g. 8 and 9·5 mol % at 1050°C and 950°C, respectively, in runs with between 4·70 and 0·89 wt % bulk H_2O content). In contrast to B1, magnetite from B2 shows a stronger X_{Usp} variation as a function of temperature. At 1050°C and 950°C, the difference in X_{Usp} between experiments with 4·50 and 0·74 wt % bulk water content is 14 and 4 mol %, respectively. MgO contents of B1 and B2 magnetite decrease with falling temperature for constant bulk water contents and with decreasing bulk water content for a given temperature. This evolution of MgO content in magnetite is related to the Mg-number of the melt. Al_2O_3 content also decreases with falling temperature for a constant bulk water content.

The ilmenite content [X_{Ilm}; calculated after Andersen *et al.* (1993)] of rhombohedral oxides synthesized in B2 decreases regularly with falling temperature (from X_{Ilm} = 43 mol % at 1050°C to X_{Ilm} = 33 mol% at 950°C for 0·74 wt % bulk water content; Table 4b) and increases systematically at constant temperature with decreasing bulk water content. The same effect of water is observed for B1 ilmenite crystallized in runs with 0·89 and 1·49 wt % bulk water content at 950°C, which have generally higher X_{Ilm} than those obtained at similar conditions in B2. Compared with magnetite, MgO, Al_2O_3, and MnO contents in ilmenite are generally lower. As for magnetite, MgO content falls with decreasing bulk water content and falling temperature.

The results of Bacon & Hirschmann (1988) can be used as a test for coexisting Fe–Ti oxide equilibrium using Mg/Mn partitioning between magnetite and ilmenite. Fe–Ti oxide pairs from B1 and B2 experiments (Table 4a and b) satisfy the Mg/Mn partitioning criterion of Bacon & Hirschmann (1988), having an average magnetite log(Mg/Mn) of 1·26 (± 0·13) and ilmenite log(Mg/Mn) of 1·40 (± 0·08).

Glass composition at MnO–Mn_3O_4 buffer conditions

Compositions of glasses obtained in B1 and B2 experiments are given in Table 4a and b and the concentrations of SiO_2 and FeO* are plotted against temperature in Figs 9 and 10. Depending on experimental conditions, glass compositions range from basaltic through dacitic to rhyolitic (run 106; classification using

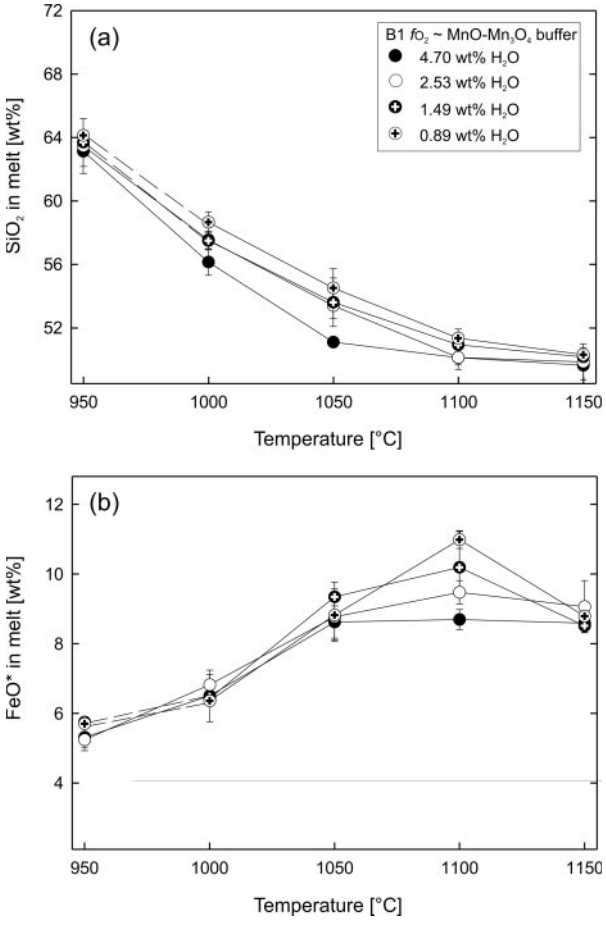

Fig. 9. B1 (MnO–Mn_3O_4 buffer) melt oxide concentrations of SiO_2 (a) and FeO* (b) (normalized to 100 wt %) as a function of bulk water content and temperature. Errors bars correspond to the standard deviation of multiple electron microprobe analyses (Table 4). All analyses are normalized to 100 wt %. Dashed lines indicate calculated melt compositions of experiments 47 and 46 (see comments in 'Analytical techniques' section).

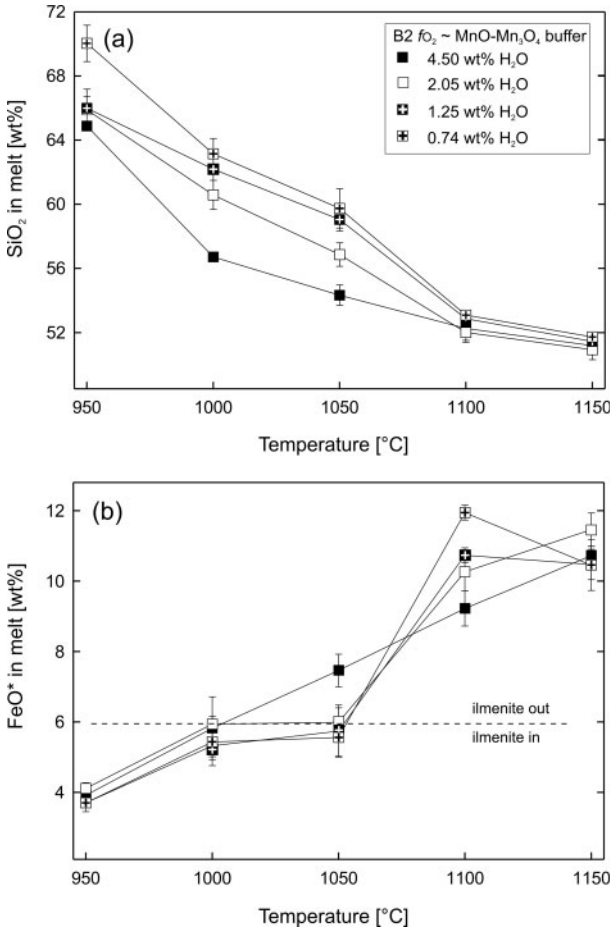

Fig. 10. B2 (MnO–Mn_3O_4 buffer) melt oxide concentrations of SiO_2 (a) and FeO* (b) (normalized to 100 wt %) as a function of bulk water content and temperature. Further details are given in the caption of Fig. 9.

the total alkalis–silica (TAS) diagram after, for example, Le Bas *et al.* (1986)] and follow a calc-alkaline differentiation trend. SiO_2, Na_2O, and K_2O concentrations continuously increase for B1 and B2 with falling temperature and decreasing bulk water content. However, compared with B2, SiO_2 contents of B1 vary only slightly for a given temperature with changing bulk water content (Figs 9a and 10a). The maximum SiO_2 concentration is about 64 wt % in B1 and 70 wt % in B2. Despite different initial Na_2O contents of B1 and B2 the same maximum Na_2O concentration of about 5·5 wt % to 4 wt % is reached in both systems for the lowest and highest bulk water contents, respectively (at 950°C).

The MgO and CaO concentrations in glasses from B1 and B2 decrease with falling temperature. In runs with high bulk water contents (4·70 and 4·50 wt % H_2O in B1 and B2, respectively), the CaO remains constant (B1) or rises slightly (B2), but decreases once clinopyroxene begins to crystallize. At constant temperature, MgO and CaO contents fall with decreasing bulk water content, in contrast to SiO_2, Na_2O and K_2O. MgO contents decrease from their initial values of 9·77 wt % (B1) and 6·49 wt % (B2) to a minimum of approximately 2·5 wt % (highest bulk water contents) and 1·2 wt % (lowest bulk water content).

The TiO_2 concentrations in B1 glasses decrease with increasing bulk water contents, which can be correlated with the increasing X_{Usp} in magnetite with increasing bulk water content (see above). For a given bulk water content TiO_2 concentrations first increase and then decrease with falling temperature. The maximum value is reached at 1100°C for 0·89 and 1·49 wt % bulk water content and at 1000°C for 2·53 and 4·70 wt % bulk water content. In B2, TiO_2 concentrations at low temperatures are mainly controlled by the crystallization of ilmenite. In

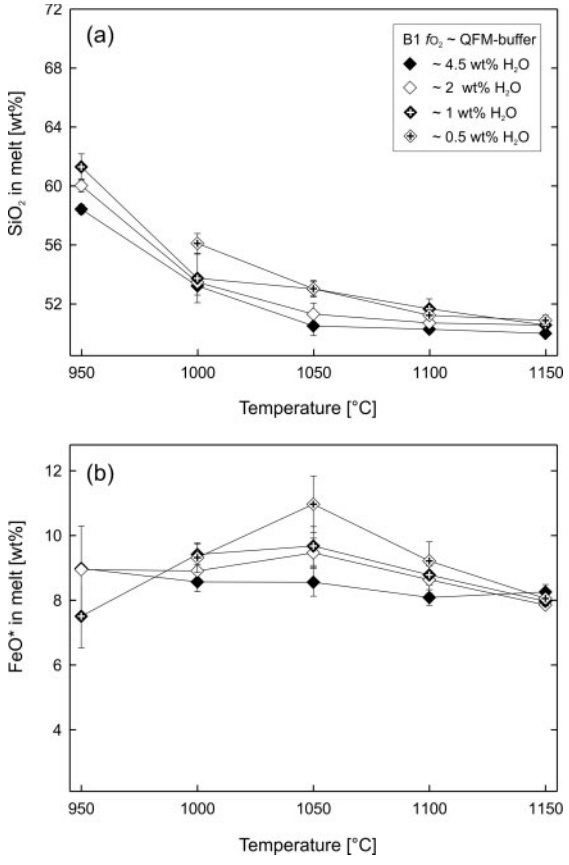

Fig. 11. B1 (QFM buffer) melt oxide concentrations of SiO_2 (a) and FeO* (b) (normalized to 100 wt %) as a function of bulk water content and temperature. Further details are given in the caption of Fig. 9.

all experiments containing ilmenite, the TiO_2 concentration in the glass is below 1·3 wt %. In addition, TiO_2 contents show a general decrease with falling bulk water content and temperature.

The evolution of FeO* content in B1 and B2 glasses is similar to that of TiO_2. In B1, the maximum FeO* values are observed at 1100°C (10·19 wt % for 1·49 wt % bulk water content; 10·98 wt % for 0·89 wt % bulk water content; Fig. 9b). The FeO* concentration in melts from experiments with 2·05 and 4·70 wt % bulk water content show only little variation down to 1050°C (about 8·9 wt %). In B2, FeO* contents of all glasses in experiments containing ilmenite are below 5·8 wt % (Fig. 10b). In addition to the effect of ilmenite, FeO* also decreases with falling temperature (for $a_{H_2O} = 1$, 4·5 wt % bulk water) and with increasing water content of the melt (compare runs at 1100°C; Fig. 10b).

Glass composition at QFM buffer conditions

Experimental melt compositions are given in Table 4c. The evolutions of melt SiO_2 and FeO* with temperature as a function of bulk water content are shown in Fig. 11. In contrast to oxidizing conditions, melts follow a tholeiitic differentiation trend (see Figs 14 and 15; Irvine & Baragar, 1971; Miyashiro, 1974), ranging from basaltic to andesitic compositions. SiO_2 content of the melt (Fig. 11a) increases with falling temperature and bulk water content up to 61 wt % (run 151). FeO* concentration generally increases with falling temperature, but shows significant variations with changing bulk water content (Fig. 11b). For water-saturated melts, FeO* content increases slightly from 1150°C to 950°C (8·24 wt % at 1150°C and 8·97 wt % at 950°C). For lower bulk water contents, FeO* first increases with falling temperature and decreases at temperatures below 1050°C. The highest FeO* is observed for about 0·5 wt % bulk water content with 10·95 wt % FeO* at 1050°C (run 143). The FeO* content in water-saturated melts at 950°C is identical in runs 153 and 152 (no ilmenite present). However, the melt FeO* content is significantly lower in run 151 containing ilmenite. With falling temperature and decreasing bulk water content, the melt MgO and CaO concentrations also decrease. In contrast, Na_2O and K_2O rise in concentration with falling temperature and bulk water content. A maximum TiO_2 content is reached at 1000°C and decreases generally in all experiments at 950°C.

DISCUSSION

Comparison of phase relations at high and low f_{O_2}

Phase relations obtained for the B1 starting composition at oxidizing and reducing oxygen fugacities can be compared to estimate the effect of f_{O_2}, as all other parameters are equal (pressure, temperature, bulk water content). For both high and low oxygen fugacities olivine is the liquidus phase crystallizing at similar temperatures between 1150°C and 1100°C, depending on bulk water content. In contrast to B1 phase relations at oxidizing conditions, orthopyroxene is not stable at low f_{O_2}. This is in agreement with previous studies (e.g. Grove & Juster, 1989), which show that decreasing melt Mg-number (as a result of decreasing f_{O_2}) strongly confines the low-Ca pyroxene stability. Because orthopyroxene is not stable at reducing conditions (melt Mg-number of about 35 at 950°C; Table 4c), olivine is present in the low-temperature runs at 950°C, in contrast to oxidizing conditions (melt Mg-number of 61–68). Magnetite did not crystallize at low f_{O_2} because of the lower melt Fe^{3+}/Fe^{2+} ratio. Ilmenite stability is known to be less dependent on the oxidation state of the melt (e.g. Toplis & Carroll, 1995), and this mineral is observed at the same temperature and bulk water contents in both reducing and oxidizing conditions. The clinopyroxene and plagioclase saturation

is also widely independent of f_{O_2}, as both phases crystallize between 1150°C and 1050°C.

Mg/Fe partitioning between olivine and melt

Partitioning of Fe and Mg between olivine and melt, expressed as $K_{D_{Fe-Mg}}^{Ol-Melt}$ (Roeder & Emslie, 1970) is known to show only a small dependence on melt composition, temperature and f_{O_2}, with a value of about 0·3 (± 0·02). The $K_{D_{Fe-Mg}}^{Ol-Melt}$ determined in this study is slightly higher with an average value of 0·33 (± 0·01). This higher value is in agreement with the results of Ulmer (1989), who showed a slight positive pressure dependence of $K_{D_{Fe-Mg}}^{Ol-Melt}$, thus suggesting that equilibrium conditions between olivine and melt have been reached in our experiments. Although $K_{D_{Fe-Mg}}^{Ol-Melt}$ is generally assumed to be constant, implying a linear relationship between X_{Fo} and melt Mg-number, it is emphasized that small but significant deviations occur as a function of the melt Mg-number. This is illustrated in Fig. 12, which shows that X_{Fo} decreases with the melt Mg-number over a wide range of bulk compositions, temperatures and oxygen fugacities. Toplis & Carroll (1995) observed, in agreement with the data of Longhi & Pan (1988) and Shi (1993), that $K_{D_{Fe-Mg}}^{Ol-Melt}$ values increase up to 0·4 for melt Mg-number <30. This has been interpreted as due to the non-ideality of Fe^{2+}–Mg mixing either in the olivine (Wiser & Wood, 1991; Toplis & Carroll, 1995) or in the melt (Hoover & Irvine, 1977), which leads to relatively lower Mg/Fe^{2+} in olivine than in the coexisting melt (Fig. 12). Our data extend the available database towards high melt Mg-number. Using this database (obtained at various P, T, a_{H_2O}, f_{O_2} and bulk compositions), we show that the equilibrium composition of olivine–liquid pairs can be described as a logarithmic function of the melt Mg-number in the pressure range 0·1–200 MPa for both dry and hydrous systems at various f_{O_2}:

$$\text{Mg-number} = \exp\left(\frac{X_{Fo} + 71{\cdot}8}{37{\cdot}54}\right). \qquad (1)$$

The curve in Fig. 12 represents the calculated X_{Fo} as a function of the liquid Mg-number using equation (1).

Effect of H_2O and f_{O_2} on olivine and orthopyroxene stability

H_2O is known to depolymerize melts and thus enhance the stability field of depolymerized phases such as olivine (e.g. Kushiro, 1975; Ulmer, 1989). The highest proportion of olivine in B1 at high f_{O_2}, calculated by mass balance, is reached at 1050°C for all bulk water contents (Table 4a). This is confirmed by the shape of the olivines. At this temperature and below, olivine textures change from euhedral to rounded crystals, indicating a partial resorption during the experiment (partial resorption of olivine is probably the result of a rapid growth of this mineral in the first minutes of the experiment when compared with the other mineral phases). Toplis & Carroll (1995) made similar observations for olivine in a dry ferrobasaltic system at slightly higher temperatures (1070–1130°C) for f_{O_2} in the range QFM + 1 to QFM – 2. Toplis & Carroll (1995) observed a falling onset temperature of olivine resorption with decreasing f_{O_2}. However, the onset of olivine resorption in our study is observed at lower temperatures despite the fact that f_{O_2} is higher in B1 runs at MnO–Mn_3O_4 buffer conditions than in the study of Toplis & Carroll (1995). A possible explanation is that the higher depolymerization of our hydrous melts leads to increasing stability and activity of olivine (e.g. Kushiro, 1975). This is supported by the study of Spulber & Rutherford (1983) showing that olivine is stable in a MORB composition until the solidus is reached at low f_{O_2} (graphite–methane buffer) and hydrous conditions ($a_{H_2O} \sim 0{\cdot}6$), suggesting that the olivine stability field is extended to lower temperatures with decreasing f_{O_2} and increasing a_{H_2O} in basaltic systems. This is also confirmed

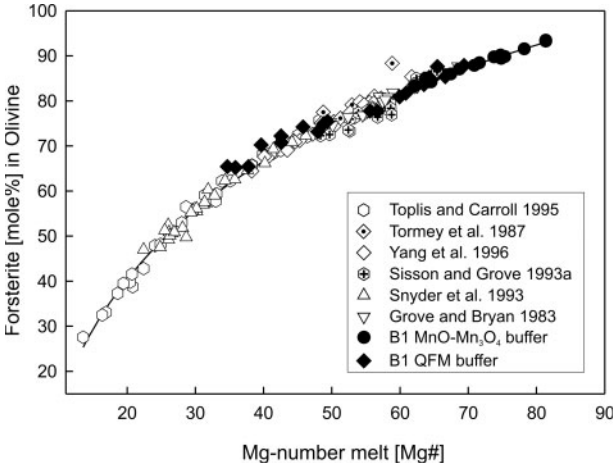

Fig. 12. Variation of forsterite content (mol % Fo) as a function of melt Mg-number (Mg#). Olivine compositions and corresponding melt Mg-number from the following studies have been added: Toplis & Carroll (1995): 1 atm, QFM + 1 to QFM – 2, 1170–1050°C, ferrobasaltic composition representing the parental liquid of the Skaergard intrusion; Tormey *et al.* (1987): only 1 atm experiments were considered, QFM, 1240–1152°C, MORB composition dredged near the Kane Fracture Zone; Yang *et al.* (1996): 1 atm, QFM, 1251–1110°C, six MORB glasses; Sisson & Grove (1993*a*): 200 MPa, NNO, H_2O saturated, 1050–925°C, high-alumina basalts; Snyder *et al.* (1993): 1 atm, QFM to 0·5 log units above iron–wüstite (IW), 1192–1061°C, ferrobasaltic compositions representing parental liquids, Newark Island layered intrusion, Kiglapait intrusion, Skaergard intrusion and a tholeiitic composition from Langjökull, Iceland; Grove & Bryan (1983): 1 atm, QFM, 1245–1131°C, four basaltic compositions (primitive basalts from the FAMOUS area, one primitive basalt characterized by 'plume-type' geochemistry and one basalt with typical parental composition near the Kane Fracture Zone). The curve is a logarithmic fit to the data for anhydrous to water-saturated basaltic systems crystallizing under low pressure (1 atm–200 MPa).

by the experiments from this study at low f_{O_2} in which olivine is always a stable phase (Fig. 4c).

As emphasized by Juster *et al.* (1989) and Toplis & Carroll (1995), high silica activities of the melt promote resorption of olivine involving a reaction of the type $Mg_2SiO_4^{ol} + SiO_2^{glass} = 2MgSiO_3^{pig}$. At high f_{O_2}, in B1 the orthopyroxene saturation curve (opx-in curve; Fig. 4a) and olivine-out curve are not identical, but overlap at 1000°C and 0·89 and 1·49 wt % bulk water content. Because the resorption of olivine roughly parallels the crystallization of orthopyroxene, we suggest that the occurrence of orthopyroxene is related to the reaction described above. Furthermore, orthopyroxene crystallizes first in runs with lower bulk water contents and thus higher crystal fraction and higher silica activity of the melts. In the fractionated B2 composition, olivine is absent. Therefore, the generally higher melt SiO_2 contents of the B2 compositions expand the stability field of orthopyroxene, particularly at low a_{H_2O} up to 1050°C.

Effect of H_2O and f_{O_2} on Fe–Ti oxide stability

The stability of Fe–Ti oxides in basaltic systems has been widely investigated because of its important influence on differentiation paths. Generally, it is difficult to discriminate between the individual effects of H_2O, f_{O_2} and melt composition (and thus activities of critical components) on the stability of ilmenite and magnetite, because a_{H_2O} also influences the prevailing f_{O_2}, which in turns controls the Fe_2O_3 content in the melt. As shown by, for example, Snyder *et al.* (1993) and Toplis & Carroll (1995), for dry basaltic systems the magnetite stability field expands to high temperature with increasing f_{O_2} (as a result of the increasing ferric iron content of the melt). In contrast, ilmenite is stable at lower f_{O_2} and is rather a function of melt TiO_2 content than of melt oxidation state (Thy & Lofgren, 1994; Toplis & Carroll, 1995). In this study, for B1 the stability field of ilmenite is identical for reducing and oxidizing conditions (Fig. 4a and c). This supports the hypothesis of Toplis & Carroll (1995) that ilmenite is nearly independent of melt oxidation state but depends mainly on melt TiO_2 content. As mentioned above, runs with low bulk water content at low temperatures have water activities less than unity despite fluid saturation having been reached in these experiments. Thus, melt fraction decreases with decreasing bulk water contents, resulting in higher TiO_2 concentrations. Therefore, at a given temperature, ilmenite stability is enhanced with decreasing bulk water content, independently of f_{O_2}. This is illustrated in Fig. 4a and c, showing that ilmenite is stable at 950°C in samples with bulk water contents between 0·55 and 1·5 wt %, but not at higher bulk water contents.

Magnetite is stable in B1 runs performed at high f_{O_2}, but not in the experiments conducted at the QFM buffer.

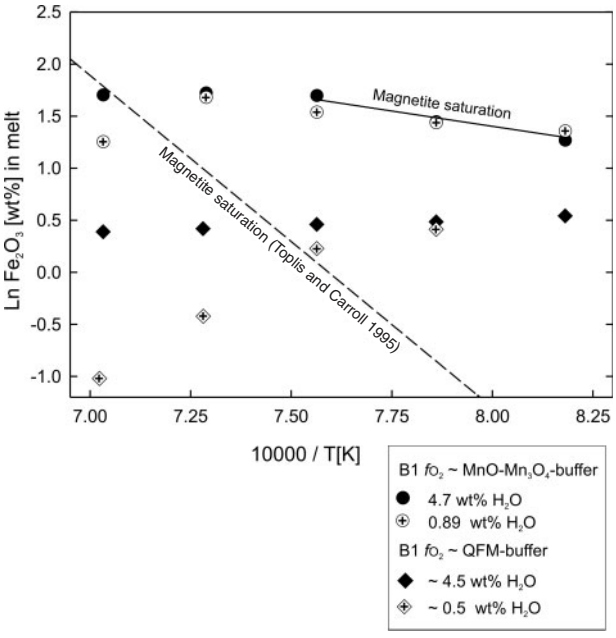

Fig. 13. Ln Fe_2O_3 content of melts as a function of the inverse temperature. Only experiments with the highest (between 4·7 and 4·5 wt %) and lowest (between ~0·5 and 0·89 wt %) bulk water contents are considered. Continuous line indicate experiments conducted at high f_{O_2} ($MnO–Mn_3O_4$ buffer) in which magnetite was a stable phase. Dashed line shows in Fe_2O_3 contents of magnetite-saturated dry melts from Toplis & Carroll (1995) for various compositions.

At high f_{O_2}, magnetite crystallizes between 1100°C and 1050°C, but is not the liquidus phase as olivine, plagioclase and clinopyroxene are stable at higher temperatures (Fig. 4a). This is in contrast to studies performed under dry conditions in basaltic systems at high f_{O_2}, in which magnetite is usually the liquidus phase, or at least a near-liquidus phase (Roeder, 1974; Grove & Juster, 1989; Juster *et al.*, 1989) with a crystallization temperature of about 1100°C (e.g. Thy & Lofgren 1994), independent of bulk composition. A possible explanation for the lower saturation temperature in hydrous MORB systems is that the solubility of magnetite is higher in hydrous melts than in dry systems. Toplis & Carroll (1995) showed [with additional data of Juster *et al.* (1989), Snyder & Carmichael (1992) and Thy & Lofgren (1994)] that the ferric iron content of magnetite-saturated liquids is a linear function of the inverse temperature for a variety of dry basaltic compositions, independently of f_{O_2} (Fig. 13). The results at high f_{O_2} show that magnetite saturation is reached at lower temperatures for a given melt Fe_2O_3 content compared with dry systems. This suggests that the activity of Fe_2O_3 in the melt is probably lowered by H_2O compared with dry systems. The absence of magnetite in B1 at the QFM buffer can be explained by the lower melt Fe_2O_3 concentration (because of the low f_{O_2}) in combination with the effect of dissolved water (Fig. 13; note that the FeO* contents are

generally higher in B1 melts obtained at low f_{O_2} than those from experiments performed under oxidizing conditions).

Differentiation trend at high and low oxygen fugacities

Residual melt compositions obtained in runs at high and low f_{O_2} allow us to estimate the influence of H_2O and f_{O_2} on the liquid line of descent, as all other parameters (bulk composition, bulk water content, temperature and pressure) were similar. The residual liquids obtained at f_{O_2} conditions corresponding to the QFM buffer show a general increase in melt FeO*/MgO ratio with falling temperature as a result of the absence of magnetite among the crystallizing phases. These melts follow, independently of bulk water content, a tholeiitic differentiation trend [Figs 14 and 15; classification after Irvine & Baragar (1971) and Miyashiro (1974)]. This is in agreement with previous studies performed in basaltic systems at lower f_{O_2}, in which Fe–Ti oxides are not stable until a significant amount of silicates crystallized and the melt is enriched in FeO* (Spulber & Rutherford, 1983; Juster *et al.*, 1989; Snyder *et al.*, 1993) following a tholeiitic differentiation trend. Residual B1 melts from experiments at high f_{O_2} coexist widely with magnetite and are consequently depleted in FeO* following a calc-alkaline differentiation trend (Figs 14 and 15). At high f_{O_2}, for the lowest bulk water contents in B1, magnetite appears 100°C or more below the liquidus (Fig. 4a). With increasing bulk water content, the magnetite appearance temperature is unaffected, but the liquidus, defined by silicates, is depressed by about 50°C (highest bulk water content). Thus, higher water contents cause magnetite to appear closer to the liquidus, as described by Sisson & Grove (1993*a*). Consequently, at MnO–Mn_3O_4 buffer conditions the liquid line of descent enters the calc-alkaline field at an earlier stage of differentiation for high bulk water contents compared with low bulk water contents (Fig. 15). At these high f_{O_2} values the potential for changing the differentiation trend with water is low, as magnetite crystallizes early and in relatively high proportions for all bulk water contents, preventing a change from a calc-alkaline to a tholeiitic trend in primitive MORBs. However, it could be expected that for oxygen fugacities corresponding to the Ni–NiO buffer, the addition of only water can change MORB differentiation path from tholeiitic (dry conditions) to calc-alkalic (water-saturated) by the early stabilization of Fe–Ti oxides under hydrous conditions, as observed for calc-alkaline systems by Sisson & Grove (1993*a*).

Mechanisms of melt FeO* enrichment during early stages of differentiation

At low as well as at high f_{O_2}, the melt FeO* content increases with falling temperature in the initial differentiation stages (Figs 9b, 10b and 11b). When comparing

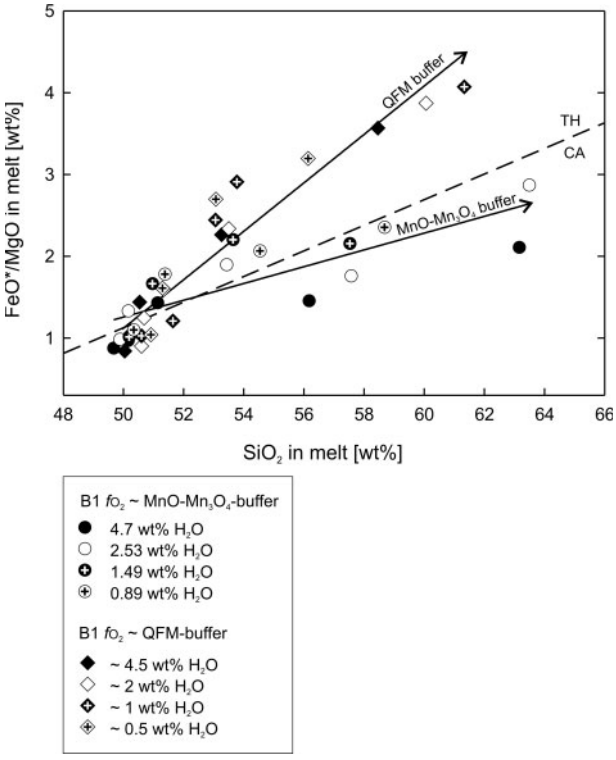

Fig. 14. FeO*/MgO ratio of residual melts vs melt SiO_2 content. TH (tholeiitic)–CA (calc-alkaline) dividing line is from Miyashiro (1974). Water contents are given as bulk water contents.

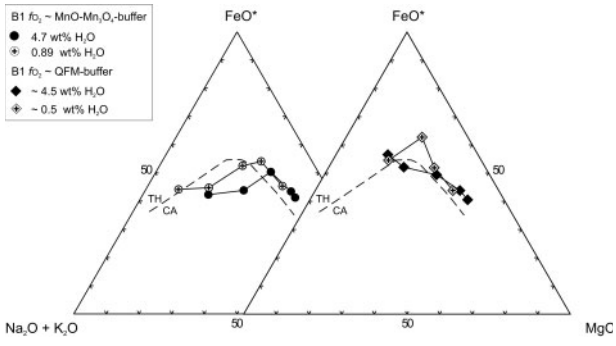

Fig. 15. Experimental residual liquids projected into the AFM, total alkali (Na_2O + K_2O)–total iron (FeO*)–MgO ternary diagram (calculated from melt composition in wt %). Only experiments with the highest (between 4·7 and 4·5 wt %) and lowest (between ~0·5 and 0·89 wt %) bulk water contents are shown. TH (tholeiitic)–CA (calc-alkaline) dividing line is from Irvine & Baragar (1971).

the melt FeO* content at a given temperature as a function of the bulk water content, the greatest differences can be observed at 1050°C at reducing conditions. At these temperatures the highest melt FeO* is obtained for the lowest bulk water content. This cannot be an effect of enhanced Fe–Ti oxide stability at high melt water contents, as magnetite is not stable under these conditions (Fig. 4c).

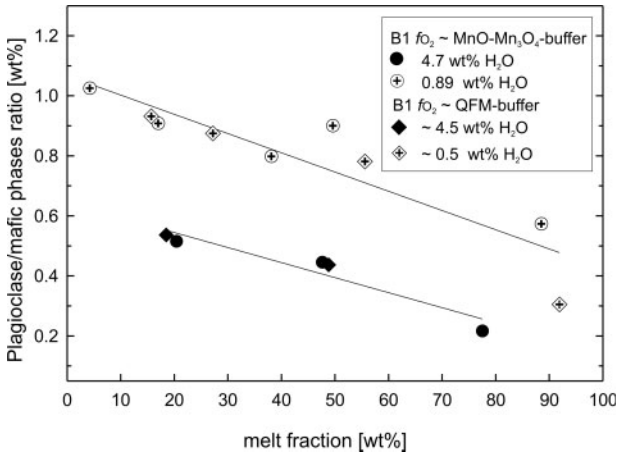

Fig. 16. Plagioclase/mafic phase ratios in B1 vs melt fraction (in wt %; both calculated by mass balance). Only experiments with the highest (between 4·7 and 4·5 wt %) and lowest (between ~0·5 and 0·89 wt %) bulk water contents are plotted.

An important factor that may control the melt FeO* enrichment during initial differentiation stages is the proportion of plagioclase and Fe–Mg silicates. As shown by, for example, Yoder (1965), Gaetani *et al.* (1993) and Sisson & Grove (1993*a*), H_2O suppresses the proportion of plagioclase as a highly polymerized phase relative to mafic Fe–Mg silicates (e.g. olivine, pyroxene, amphibole). Thus, crystallization of higher proportions of Fe–Mg silicates and destabilization of plagioclase at high water contents depletes the melt in Fe and Mg. The plagioclase/Fe–Mg-silicate ratio is shown in Fig. 16 for the highest and lowest bulk water contents at oxidizing and reducing conditions, respectively. As expected, the plagioclase/Fe–Mg-silicate ratio is significantly higher in runs with low bulk water content and independent of the f_{O_2}. Consequently, residual melts obtained from experiments performed at low water contents should show systematically higher melt FeO* concentrations than more hydrous liquids. However, this is the case only for those runs conducted at high temperatures; it is not observed for the low-temperature runs, as melt FeO* concentrations are almost similar at a temperature of 1000°C (Figs 9b, 10b and 11b). It should be noted that the composition of the melt, and thus its FeO* content, is not only dependent on the ratio of plagioclase/mafic minerals in combination with Fe–Ti-oxide crystallization, as magnetite is not stable in the low-f_{O_2} runs (Fig. 4c), but is also a complex function of the proportion and composition of clinopyroxene and olivine, which vary with water content. At 950°C the FeO* enrichment process is even reversed compared with the high-temperature situation: the residual melt obtained from experiments performed at low bulk water content (1 wt % H_2O) shows the lowest FeO* concentration. This is obviously due to the presence of ilmenite in combination with a very low melt fraction (7·9 wt %) in this run driving the FeO* content in the melt to lower values (Table 3c, Fig. 11b).

Fractionation effects

A perfect fractional crystallization path requires a continuous removal of solids from the system. In our study we have investigated two compositions at high f_{O_2}, B1 and B2, where B2 corresponds to the composition of the residual melt of a run in the B1 system after 50 wt % crystallization and a bulk water content of 0·89 wt % (run 42, Table 3a). Thus, only one fractionation step has been carried out. This fractionation event is far from being representative of natural fractionation steps but illustrates the influence of fractionation on liquid line of descent and phase relations.

Experimental results from the evolved B2 composition show that phase relations are different from B1 (Fig. 4a and b). Magnetite is the liquidus phase in B2 because of the high f_{O_2} and the melt Fe_2O_3 content, which is higher than in B1. Stability fields of both orthopyroxene and ilmenite are enhanced as a result of the higher a_{SiO_2} and of generally higher melt TiO_2 concentration, respectively. The curves of equal a_{H_2O} are shifted to lower temperatures because of the generally lower crystal fraction in B2 (Fig. 4b). Mineral and melt compositions produced in B2 are different from those in B1 and are consistent with equilibrium compositions in more evolved systems. Our results also show that starting with a primitive MORB, a quartz andesitic melt can be obtained without any fractionation step (e.g. B1, 12·6% melt, run 48), and a rhyolitic–trondhjemitic melt can already be obtained after one fractionation step (B2, 14% melt, run 106).

Implications for the origin of SiO_2-rich residual melts in MORB systems

Always included in the MORB-derived gabbroic section of the oceanic crust are small, but ubiquitous, amounts of felsic, evolved rocks, the so-called oceanic plagiogranites (e.g. Dick *et al.*, 1991). Such rocks are commonly found in ophiolites (e.g. Coleman & Peterman, 1975; Malpas, 1979; Jenner *et al.*, 1991). The processes discussed to generate these SiO_2-rich melts are: (1) crystal–liquid differentiation from a basaltic magma (e.g. Arth *et al.*, 1978; Pedersen & Malpas, 1984; Martin, 1987; Niu *et al.*, 2002); (2) partial melting of gabbro, basalt, or amphibolite (e.g. Flagler & Spray, 1991; Springer & Seck, 1997); (3) immiscibility between an Fe-enriched and a silicic residual liquid (Dixon & Rutherford, 1979). There is, however, no evidence in the experiments that residual melts become immiscible at later stages of differentiation. SiO_2-rich residual melts containing more than 60 wt %

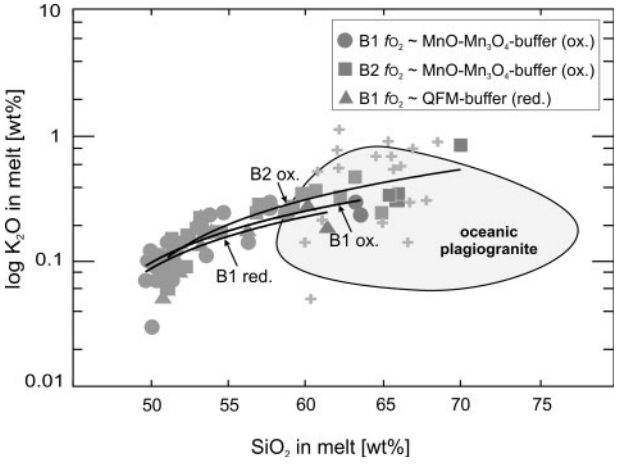

Fig. 17. Liquid lines of descent in log K_2O vs SiO_2 (wt %) (normalized to a total of 100 wt %; all bulk water contents are included) for B1 and B2 at QFM and MnO–Mn_3O_4 buffer conditions. +, natural plagiogranites from different tectonic settings (see Koepke *et al.* 2004, table 4). Included is the field for oceanic plagiogranites after Coleman & Donato (1979).

SiO_2 are produced in the B1 crystallization experiments under oxidizing and reducing f_{O_2} conditions at 950°C (Fig. 14). As expected, the B1 residual liquids obtained under high f_{O_2} are more SiO_2 rich than those at reducing conditions, as a result of the crystallization of magnetite at high f_{O_2}, which causes a stronger SiO_2 enrichment of the melt (e.g. Toplis & Carroll, 1995; about 64 wt % SiO_2 in residual melts at the MnO–Mn_3O_4 buffer and about 60 wt % SiO_2 in melts at the QFM buffer at 950°C). Thus, residual melts at 950°C are plagiogranitic in terms of SiO_2 and K_2O, as natural plagiogranites have bulk SiO_2 contents between 60 and 75 wt % (e.g. Coleman & Peterman, 1975; Fig. 17). Compared with natural plagiogranite compositions (see Koepke *et al.*, 2004, table 4) the Ca-numbers [$100 \times X_{CaO}/(X_{CaO} + X_{NaO0{\cdot}5})$] of the experimental melts of primitive B1 are very high, implying that potential plagioclase crystallizing in these liquids would be too An rich. The Ca-number values of the plagiogranitic melts of the more fractionated B2 starting composition match those found in natural plagiogranite compositions, indicating that fractionation processes need to be involved to reach the typical Ab-rich plagioclases of natural plagiogranites and also the high bulk SiO_2 contents (>70 wt %) of some natural rocks.

However, typical bulk FeO* contents in plagiogranites are in the range of 1–7 wt %, which does not match values for the liquids obtained under QFM buffer conditions as a result of the tholeiitic differentiation trend caused by the absence of magnetite (with about 9 wt % melt FeO* content in the most evolved melts of B1; Fig. 11b). In contrast, residual liquids produced under oxidizing conditions show melt FeO* contents of about 5 wt %, corresponding to common bulk iron contents found in natural plagiogranites. This does, however, not mean that generation of plagiogranites takes place at such high f_{O_2}. Fractionation of B1 at the QFM buffer would also result in FeO* depletion and SiO_2 enrichment of the melt as soon as the crystallization temperature of magnetite is reached. It can be noted that this temperature is significantly lower at QFM than at MnO–Mn_3O_4 buffer conditions. As reported by Dick *et al.* (2000) and Desmurs *et al.* (2002), there is indeed evidence for Fe–Ti-oxide fractionation in natural MORB systems, which is apparently required to produce plagiogranites with typical FeO* contents of about 5 wt %.

CONCLUSIONS

H_2O and f_{O_2} are found to be important factors in controlling solid phase compositions and stability in a MORB system. It has been demonstrated that changing a_{H_2O} influences significantly the Mg/Fe ratio in iron-bearing phases such as olivine as a result of changing f_{O_2}. Furthermore, increasing a_{H_2O} influences Fe–Ti oxide compositions by raising the f_{O_2} of the charge. $K_{D_{Ca-Na}}^{Pl-Melt}$ values for plagioclase obtained in this study for a given melt water content agree well with previous studies (e.g. Sisson & Grove, 1993*a*), confirming that plagioclase composition mainly depends on the melt water content and the Ca/Na ratio of the system.

At QFM buffer conditions the residual melt FeO*/MgO ratio generally increases with falling temperature following a tholeiitic differentiation trend. A calc-alkaline differentiation trend is observed at high f_{O_2} (MnO–Mn_3O_4 buffer), as magnetite crystallizes between 1100°C and 1050°C, independently of bulk water content. However, the crystallization temperature of silicates is depressed with increasing bulk water content. Thus, residual melts of runs with high bulk water contents show a more distinct calc-alkaline differentiation trend, even though the effect is small at these high oxygen fugacities and no change from calc-alkaline to tholeiitic trend can be produced by lowering the water content. This is probably the case in the investigated MORB system at oxygen fugacities relevant to arc magmas (Ni–NiO), as proposed by Sisson & Grove (1993*a*) for calc-alkaline systems, in which the addition of H_2O favours a calc-alkaline differentiation trend by early stabilization of Fe–Ti oxides. In addition to f_{O_2} and H_2O, which influence melt FeO* evolution by stabilization of Fe–Ti oxides, water controls melt iron content also by the plagioclase/Fe–Mg-silicate ratio in the main crystallization interval.

Phase relations, crystallization sequence and mineral compositions obtained from evolved melt compositions of MORB systems after 50 wt % crystallization are different from the primitive MORB composition. In detail, the

liquid lines of descent differ slightly (higher SiO_2 contents of melts are reached at identical P, T and a_{H_2O}). However, the general compositional trends of residual melts obtained in both compositions are very similar. SiO_2-rich residual melts can be obtained under both oxidizing and reducing conditions but at least one fractionation step is required to reach plagiogranitic residual melt compositions.

ACKNOWLEDGEMENTS

We thank Otto Dietrich for preparing the samples, and Bettina Aichinger and Willi Hurkuck for technical assistance. Harald Behrens and Marcus Nowak are thanked for many helpful discussions. Reviews by Othmar Müntener, Fidel Costa, Tom Sisson and Leonid Danyushevsky have significantly improved the manuscript. The authors also thank Colin W. Devey for editorial handling. This study was supported by Deutsche Forschungsgemeinschaft grant (project no. KO 1723/1).

REFERENCES

Andersen, D. J., Lindsley, D. H. & Davidson, P. M. (1993). QUILF: a PASCAL program to assess equilibria among Fe–Mg–Ti-oxides, pyroxenes, olivine and quartz. *Computational Geosciences* **19**, 1333–1350.

Arth, J. G., Barker, F., Peterman, Z. E. & Friedman, I. (1978). Geochemistry of the gabbro–diorite–tonalite–trondhjemite suite of tonalite and trondhjemite magmas. *Journal of Petrology* **19**, 289–316.

Bacon, C. R. & Hirschmann, M. M. (1988). Mg/Mn partitioning as a test for equilibrium between coexisting Fe–Ti oxides. *American Mineralogist* **73**, 57–61.

Baker, D. R. & Eggler, D. H. (1987). Compositions of anhydrous and hydrous melts coexisting with plagioclase, augite, and olivine or low-Ca pyroxene from 1 atm to 8 kbar: application to the Aleutian volcanic center of Atka. *American Mineralogist* **72**, 12–28.

Baker, L. L. & Rutherford, M. J. (1996). The effect of dissolved water on the oxidation state of silicic melts. *Geochimica et Cosmochimica Acta* **60**, 2179–2187.

Behrens, H. (1995). Determination of water solubilities in high-viscosity melts—an experimental study on $NaAlSi_3O_8$ and $KAlSi_3O_8$ melts. *European Journal of Mineralogy* **7**, 905–920.

Berndt, J., Holtz, F. & Koepke, J. (2001). Experimental constraints on storage conditions in the chemically zoned phonolitic magma chamber of the Laacher See volcano. *Contributions to Mineralogy and Petrology* **140**, 469–486.

Berndt, J., Liebske, C., Holtz, F., Freise, M., Nowak, M., Ziegenbein, D., Hurkuck, W. & Koepke, J. (2002). A combined rapid-quench and H_2-membrane setup for internally heated pressure vessels: description and application for water solubility in basaltic melts. *American Mineralogist* **87**, 1717–1726.

Brooks, C. K., Larsen, L. M. & Nielsen, T. F. D. (1991). Importance of iron-rich tholeiitic magmas at divergent plate margins: a reappraisal. *Geology* **19**, 269–272.

Bryan, W. B. & Moore, J. G. (1977). Compositional variations of young basalts in the Mid Atlantic Ridge rift valley near lat. 36°49′N. *Geological Society of America Bulletin* **88**, 556–570.

Burnham, C. W. (1979). The importance of volatile constituents. In: Yoder, H. D. (ed.) *Evolution of Igneous Rocks*. Princeton, NJ: Princeton University Press, pp. 439–482.

Carmichael, I. S. E. & Ghiorso, M. S. (1986). Oxidation–reduction relations in basic magma: a case for homogeneous equilibria. *Earth and Planetary Science Letters* **78**, 200–210.

Carmichael, I. S. E., Turner, F. J. & Verhoogen, J. (1974). *Igneous Petrology*. Berkeley, CA: University of California.

Chou, I.-M. (1978). Calibration of oxygen buffers at elevated P and T using the hydrogen fugacity sensor. *American Mineralogist* **63**, 690–703.

Christie, D. M. & Sinton, J. M. (1986). Major elements constraints on melting, differentiation and mixing of magmas from the Galapagos 95·5°W propagating rift system. *Contributions to Mineralogy and Petrology* **94**, 274–288.

Christie, D. M., Carmichael, I. S. E. & Langmuir, C. H. (1986). Oxidation state of mid-ocean ridge basalt glasses. *Earth and Planetary Science Letters* **79**, 397–411.

Coleman, R. G. & Donato, M. M. (1979). Oceanic plagiogranite revisited. In: Barker, F. (ed.) *Trondhjemites, Dacites and Related Rocks*. Amsterdam: Elsevier, pp. 149–167.

Coleman, R. G. & Peterman, Z. E. (1975). Oceanic plagiogranite. *Journal of Geophysical Research* **80**, 1099–1108.

Coogan, L. A., Wilson, R. N., Gillis, K. M. & MacLeod, C. J. (2001). Near-solidus evolution of oceanic gabbros: insights from amphibole geochemistry. *Geochimica et Cosmochimica Acta* **65**(23), 4339–4357.

Danyushevsky, L. V., Eggins, S. M., Falloon, T. J. & Christie, D. M. (2000). H_2O abundance in depleted to moderately enriched mid-ocean ridge magmas; Part I: Incompatible behaviour, implications for mantle storage, and origin of regional variations. *Journal of Petrology* **41**, 1329–1364.

Desmurs, L., Müntener, O. & Manatschal, G. (2002). Onset of magmatic accretion within a magma-poor rifted margin; a case study from the Platta ocean–continent transition, eastern Switzerland. *Contributions to Mineralogy and Petrology* **144**, 365–382.

Devine, J. D., Gardner, J. E., Brack, H. P., Layne, G. D. & Rutherford, M. J. (1995). Comparison of microanalytical methods for estimating H_2O contents of silicic volcanic glasses. *American Mineralogist* **80**, 319–328.

Dick, H. J. B., Meyer, P. S., Bloomer, S., Kirby, S., Stakes, D. & Mawer, C. (1991). Lithostratigraphic evolution of an in-situ section of oceanic layer 3^1. In: Von Herzen, R. P., Robinson, P. T., Fox, J. & Palmer-Julson, A. (eds) *Proceedings of the Ocean Drilling Program: Scientific Results, 118*. College Station, TX: Ocean Drilling Program, pp. 439–538.

Dick, H. J. B., Natland, J. H., Alt, J. C., *et al.* (2000). A long *in situ* section of the lower ocean crust: results of ODP Leg 176 drilling at the Southwest Indian Ridge. *Earth and Planetary Science Letters* **179**, 31–51.

Dixon, S. & Rutherford, M. J. (1979). Plagiogranites as late-stage immiscible liquids in ophiolite and mid-ocean ridge suites: an experimental study. *Earth and Planetary Science Letters* **45**, 45–60.

Elthon, D. (1991). Experimental phase petrology of mid-ocean ridge basalts. In: Floyd, P. A. (ed.) *Oceanic Basalts*. Glasgow: Blackie, pp. 94–115.

Fisk, M. R. (1984). Depths and temperatures of mid-ocean-ridge magma chambers and the composition of their source magmas. In: Gass, I. G., Lippard, S. J. & Shelton, A. W. (eds) *Ophiolites and Oceanic Lithosphere. Geological Society, London, Special Publications* **13**, 17–23.

Flagler, P. A. & Spray, J. G. (1991). Generation of plagiogranite by amphibolite anatexis in oceanic shear zones. *Geology* **19**, 70–73.

Ford, C. E. (1978). Platinum–iron alloy sample containers for melting experiments on iron-bearing rocks, minerals, and related systems. *Mineralogical Magazine* **42**, 271–275.

Frey, F. A., Bryan, W. B. & Thompson, G. (1974). Atlantic Ocean floor, geochemistry and petrology of basalts from leg 2 and 3 of the Deep Sea Drilling Project. *Journal of Geophysical Research* **79**, 5507–5527.

Gaetani, G. A. & Grove, T. L. (1998). The influence of water on melting of mantle peridotite. *Contributions to Mineralogy and Petrology* **131**, 323–346.

Gaetani, G. A., Grove, T. L. & Bryan, W. B. (1993). The influence of water on the petrogenesis of subduction-related igneous rocks. *Nature* **365**, 332–335.

Gaillard, F., Scaillet, B., Pichavant, M. & Beny, J. L. (2001). The effect of water and f_{O_2} on the ferric–ferrous ratio of silicic melts. *Chemical Geology* **174**, 255–273.

Gardien, V., Thompson, A. B., Grujic, G. & Ulmer, P. (1995). Experimental melting of biotite + plagioclase + quartz ± muscovite assemblages and implications for crustal melting. *Journal of Geophysical Research* **100**, 15581–15591.

Gillis, K. M. (1996). Rare earth element constraints on the origin of amphibole in gabbroic rocks from site 894, Hess Deep. In: Mével, C., Gillis, K. M., Allan, J. F. & Meyer, P. S. (eds) *Proceedings of the Ocean Drilling Program, Scientific Results, 147*. College Station, TX: Ocean Drilling Program, pp. 21–58.

Grove, T. L. & Baker, M. B. (1984). Phase equilibrium controls on the tholeiitic versus calc-alkaline differentiation trends. *Journal of Geophysical Research* **89**, 3253–3274.

Grove, T. L. & Bryan, W. B. (1983). Fractionation of pyroxene-phyric MORB at low pressure: an experimental study. *Contributions to Mineralogy and Petrology* **84**, 293–309.

Grove, T. L. & Juster, T. C. (1989). Experimental investigations of low-Ca pyroxene stability and olivine–pyroxene–liquid equilibria at 1-atm in natural basaltic and andesitic liquids. *Contributions to Mineralogy and Petrology* **103**, 287–305.

Hamilton, D. L., Burnham, C. W. & Osborn, E. F. (1964). The solubility of water and effects of oxygen fugacity and water content on crystallization in mafic magmas. *Journal of Petrology* **5**, 21–39.

Helz, R. T. (1973). Phase relations of basalts in their melting range at $PH_2O = 5$ kb as a function of oxygen fugacity. Part I. Mafic phases. *Journal of Petrology* **14**, 249–302.

Helz, R. T. (1976). Phase relations of basalts in their melting range at $PH_2O = 5$ kb. Part II. Melt compositions. *Journal of Petrology* **17**, 139–193.

Helz, R. T. (1981). Phase relations and compositions of amphiboles produced in studies of the melting behavior of rocks. In: Ribbe, P. H. & Veblen, D. R. (eds) *Amphiboles: Petrology and Experimental Phase Relations. Mineralogical Society of America, Reviews in Mineralogy* **9B**, 279–353.

Holloway, J. R. & Burnham, C. W. (1972). Melting relations of basalt with equilibrium water pressure less than total pressure. *Journal of Petrology* **13**, 1–29.

Holloway, J. R., Dixon, J. E. & Pawley, A. R. (1992). An internally heated, rapid-quench, high-pressure vessel. *American Mineralogist* **77**, 643–646.

Holtz, F., Behrens, H., Dingwell, D. B. & Johannes, W. (1995). H_2O solubility in haplogranitic melts—compositional, pressure, and temperature-dependence. *American Mineralogist* **80**, 94–108.

Hoover, J. D. & Irvine, T. N. (1977). Liquidus relations and Mg–Fe partitioning on part of the system Mg_2SiO_4–Fe_2SiO_4–$CaMgSi_2O_6$–$CaFeSi_2O_6$–$KAlSi_3O_8$–SiO_2. *Carnegie Institution of Washington Yearbook* **77**, 774–784.

Irvine, T. N. & Baragar, W. R. A. (1971). A guide to chemical classification of the common volcanic rocks. *Canadian Journal of Earth Science* **8**, 523–548.

Jenner, G. A., Dunning, G. R., Malpas, J., Brown, M. & Brace, T. (1991). Bay of Islands and Little Port complexes, revisited: age, geochemical and isotopic evidence confirm suprasubduction-zone origin. *Canadian Journal of Earth Science* **28**, 1635–1652.

Johannes, W. & Bode, B. (1978). Loss of iron to the Pt-container in melting experiments with basalts and a method to reduce it. *Contributions to Mineralogy and Petrology* **67**, 221–225.

Johnson, M. C., Andersen, A. T. J. & Rutherford, M. J. (1994). Pre-eruptive volatile contents of magmas. In: Carroll, M. R. & Holloway, J. R. (eds) *Volatiles in Magmas. Mineralogical Society of America, Reviews in Mineralogy* **30**, 281–330.

Jurewicz, A. J. G. & Watson, E. B. (1988). Cations in olivine, Part 1: Calcium partitioning and calcium–magnesium distribution between olivines and coexisting melts, with petrologic applications. *Contributions to Mineralogy and Petrology* **99**, 176–185.

Juster, T. C., Grove, T. L. & Perfit, M. R. (1989). Experimental constraints on the generation of FeTi basalts, andesites, and rhyodacites at the Galapagos Spreading Center, 85°W and 95°W. *Journal of Geophysical Research* **94**, 9251–9274.

Kawamoto, T. (1996). Experimental constraints on differentiation and H_2O abundance of calc-alkaline magmas. *Earth and Planetary Science Letters* **144**, 577–589.

Kawamoto, T. & Hirose, K. (1994). Au–Pd sample containers for melting experiments on iron and water bearing systems. *European Journal of Mineralogy* **6**, 381–385.

Koepke, J. (1997). Analyse von wasserhaltigen silikatischen Gläsern mit der Mikrosonde: Wassergehalte und Alkalienverluste. *Berichte der Deutschen Mineralogischen Gesellschaft, Beiheft in European Journal of Mineralogy* **9**, 200.

Koepke, J., Johannes, W. & Becker, A. (1996). Determination of crystal/melt fractions with the help of BSE-pictures and image analysis. *Terra Nova, Abstract Supplement* **8**, 36.

Koepke, J., Feig, S. T., Snow, J. & Freise, M. (2004). Petrogenesis of oceanic plagiogranites by partial melting of gabbros: an experimental study. *Contributions to Mineralogy and Petrology* **146**, 414–432.

Kovalenko, V. I., Naumov, V. B., Yarmolyuk, V. V. & Dorofeeva, V. A. (2000). Volatile components (H_2O, CO_2, Cl, F, and S) in magmas of intermediate and acid compositions from distinct geodynamic settings: evidence from melt inclusions and chill glasses. *Petrology* **8**, 525–556.

Kress, V. C. & Carmichael, I. S. E. (1991). The compressibility of silicate liquids containing Fe_2O_3 and the effect of composition, temperature, oxygen fugacity and pressure on their redox states. *Contributions to Mineralogy and Petrology* **108**, 82–92.

Kushiro, I. (1975). On the nature of silicate melts and its significance in magma genesis: regularities in the shift of liquidus boundaries involving olivine, pyroxene, and silica materials. *American Journal of Science* **275**, 411–432.

Lange, R. A. (1997). A revised model for the density and thermal expansivity of K_2O–Na_2O–CaO–MgO–Al_2O_3–SiO_2 liquids from 700 to 1900 K: extension to crustal magmatic temperatures. *Contributions to Mineralogy and Petrology* **130**, 1–11.

Lange, R. A. & Carmichael, I. S. E. (1990). Thermodynamic properties silicate liquids with emphasis on density, thermal expansion and compressibility. In: Ribbe, P. H. (ed.) *Modern Methods of Igneous Petrology: Understanding Magmatic Processes. Mineralogical Society of America, Reviews in Mineralogy* **24**, 25–64.

Langmuir, C. H., Bender, J. F., Bence, A. E. & Hanson, G. N. (1977). Petrogenesis of basalt from the FAMOUS area, Mid-Atlantic Ridge. *Earth and Planetary Science Letters*, **36**, 133–156.

Le Bas, M. J., Le Maitre, R. W., Streckeisen, A. & Zanettin, B. (1986). A chemical classification of volcanic rocks based on the total alkali–silica diagram. *Journal of Petrology* **27**, 745–750.

Leake, B. E., Woolley, A. R., Birch, W. D., *et al.* (1997). Nomenclature of amphiboles—Report of the Subcommittee on Amphiboles of the International Mineralogical Association Commission on New Minerals and Mineral Names. *European Journal of Mineralogy* **9**, 623–651.

Libourel, G. (1999). Systematics of calcium partitioning between olivine and silicate melt: implications for melt structure and calcium content of magmatic olivines. *Contributions to Mineralogy and Petrology* **136**, 63–80.

Longhi, J. & Pan, V. (1988). A reconnaisance study of phase boundaries in low-alkali basaltic liquids. *Journal of Petrology* **29**, 115–147.

Longhi, J., Walker, D. & Hays, J. F. (1978). The distribution of Fe and Mg between olivine and lunar basaltic liquids. *Geochimica et Cosmochimica Acta* **42**, 1545–1558.

Malpas, J. (1979). Two contrasting trondhjemite associations from transported ophiolites in western Newfoundland: initial report. In: Barker, F. (ed.) *Trondhjemites, Dacites, and Related Rocks*. Amsterdam: Elsevier, pp. 465–484.

Martel, C., Pichavant, M., Bourdier, J.-L., Traineau, H., Holtz, F. & Scaillet, B. (1998). Magma storage conditions and control of eruption regime in silicic volcanoes: experimental evidence from Mt. Pelee. *Earth and Planetary Science Letters* **156**, 89–99.

Martin, H. (1987). Petrogenesis of Archean trondhjemites, tonalites, and granodiorites from Eastern Finland: major and trace element geochemistry. *Journal of Petrology* **28**, 921–953.

McKenzie, D. P. & Bickle, M. J. (1988). The volume and composition of melt generated by extension of the lithosphere. *Journal of Petrology* **29**, 625–679.

Miyashiro, A. (1974). Volcanic rock series in island arcs and active continental margins. *American Journal of Science* **274**, 321–355.

Müntener, O., Kelemen, P. B. & Grove, T. L. (2001). The role of H_2O during crystallization of primitive arc magmas under uppermost mantle conditions and genesis of igneous pyroxenites: an experimental study. *Contributions to Mineralogy and Petrology* **141**, 643–658.

Natland, J. H. & Melson, W. G. (1980). Compositions of basaltic glasses from the East Pacific Rise and the Siqueiros Fracture Zone, near 9°. In: Rosendahl, B. R. (ed.) *Initial Reports of the Deep Sea Drilling Project, Vol. 54*. Washington, DC: US Government Printing Office, pp. 705–723.

Nicolas, A. (1989). *Structures of Ophiolites and Dynamics of Oceanic Lithosphere*. Dordrecht: Kluwer Academic.

Niu, Y., Gilmore, T., Mackie, S., Greig, A. & Bach, W., 2002. Mineral chemistry, whole-rock compositions, and petrogenesis of Leg 176 gabbros: data and discussion. In: Natland, J. H., Dick, H. J. B., Miller, D. J. & Von Herzen, R. P. (eds) *Proceedings of the Ocean Drilling Program, Scientific Results, 176*. College Station, TX: Ocean Drilling Program, pp. 1–60 [Online]. Available at http://www-odp.tamu.edu/publications/176_SR/VOLUME/CHAPTERS/SR176_08.PDF. Accessed 3 November 2003.

Ochs, F. A., III & Lange, R. A. (1999). The density of hydrous magmatic liquids. *Science* **283**, 1314–1317.

Osborn, E. F. (1959). Role of oxygen pressure in the crystallization and differentiation of basaltic magma. *American Journal of Science* **257**, 609–647.

Panjasawatwong, Y., Danyushevsky, L. V., Crawford, A. J. & Harris, K. L. (1995). An experimental study of the effects of melt composition on plagioclase–melt equilibria at 5 and 10 kbar: implications for the origin of magmatic high-An plagioclase. *Contributions to Mineralogy and Petrology* **118**, 420–432.

Pedersen, R. B. & Malpas, J. (1984). The origin of oceanic plagiogranites from the Karmoy ophiolite, Western Norway. *Contributions to Mineralogy and Petrology* **88**, 36–52.

Pichavant, M. (1987). Effects of B and H_2O on liquidus phase relations in the haplogranite system at 1 kbar. *American Mineralogist* **72**, 11–12.

Roeder, P. L. (1974). Activity of iron and olivine solubility in basaltic liquids. *Earth and Planetary Science Letters* **23**, 397–410.

Roeder, P. L. & Emslie, R. F. (1970). Olivine–liquid equilibrium. *Contributions to Mineralogy and Petrology* **29**, 275–289.

Roux, J. & Lefevre, A. (1992). A fast-quench device for internally heated pressure vessels. *European Journal of Mineralogy* **4**, 279–281.

Scaillet, B. & Evans, B. W. (1999). The 15 June 1991 eruption of Mount Pinatubo. I. Phase equilibria and pre-eruption P–T–fO_2–fH_2O conditions of the dacite magma. *Journal of Petrology* **40**, 381–411.

Scaillet, B., Pichavant, M. & Roux, J. (1995). Experimental crystallization of leucogranite magmas. *Journal of Petrology* **36**, 663–705.

Schwab, R. G. & Küstner, D. (1981). The equilibrium fugacities of important oxygen buffers in technology and petrology. *Neues Jahrbuch für Mineralogie* **140**, 112–142.

Shi, P. (1993). Low-pressure phase relationships in the system Na_2O–CaO–FeO–MgO–Al_2O_3–SiO_2 at 1100°C, with implications for the differentiation of basaltic magmas. *Journal of Petrology* **34**, 743–762.

Sisson, T. W. & Grove, T. L. (1993*a*). Experimental investigations of the role of H_2O in calc-alkaline differentiation and subduction zone magmatism. *Contributions to Mineralogy and Petrology* **113**, 143–166.

Sisson, T. W. & Grove, T. L. (1993*b*). Temperatures and H_2O contents of low-MgO high-alumina basalts. *Contributions to Mineralogy and Petrology* **113**, 167–184.

Snyder, D. A. & Carmichael, I. S. E. (1992). Olivine–liquid equilibria and the chemical activities of FeO, NiO, Fe_2O_3, and MgO in natural basic melts. *Geochimica et Cosmochimica Acta* **56**, 303–318.

Snyder, D., Carmichael, M. J. & Wiebe, R. A. (1993). Experimental study of liquid evolution in an Fe-rich, layered mafic intrusion: constraints of Fe–Ti oxide precipitation on the T–f_{O_2} and T–DELTA paths of tholeiitic magmas. *Contributions to Mineralogy and Petrology* **113**, 73–86.

Sobolev, A. V. & Chaussidon, M. (1996). H_2O concentrations in primary melts from supra-subduction zones and mid-ocean ridges: implications for H_2O storage and recycling in the mantle. *Earth and Planetary Science Letters* **137**, 45–55.

Springer, W. & Seck, H. A. (1997). Partial fusion of basic granulites at 5 to 15 kbar: implications for the origin of TTG magmas. *Contributions to Mineralogy and Petrology* **127**, 30–45.

Spulber, S. D. & Rutherford, M. J. (1983). The origin of rhyolite and plagiogranite in oceanic crust: an experimental study. *Journal of Petrology* **24**, 1–25.

Taylor, J. R., Wall, V. J. & Pownceby, M. I. (1992). The calibration and application of accurate redox sensors. *American Mineralogist* **77**, 284–295.

Thy, P. & Lofgren, G. E. (1994). Experimental constraints on the low-pressure evolution of transitional and mildly alkalic basalts: the effect of Fe–Ti oxide minerals and the origin of basaltic andesites. *Contributions to Mineralogy and Petrology* **116**, 340–351.

Toplis, M. J. & Carroll, M. R. (1995). An experimental study of the influence of oxygen fugacity on Fe–Ti oxide stability, phase relations, and mineral–melt equilibria in ferro-basaltic systems. *Journal of Petrology* **36**, 1137–1170.

Toplis, M. J. & Carroll, M. R. (1996). Differentiation of ferro-basaltic magmas under conditions open and closed to oxygen: implications

for the Skaergaard Intrusion and other natural systems. *Journal of Petrology* **37**, 837–858.

Tormey, D. R., Grove, T. L. & Bryan, W. B. (1987). Experimental petrology of normal MORB near the Kane Fracture Zone: 22°–25° N, Mid-Atlantic Ridge. *Contributions to Mineralogy and Petrology* **96**, 121–139.

Turner, F. J. & Verhoogen, J. (1960). *Igneous and Metamorphic Petrology*. New York: McGraw–Hill.

Ulmer, P. (1989). The dependence of the Fe^{2+}–Mg cation-partitioning between olivine and basaltic liquid on pressure, temperature and composition. *Contributions to Mineralogy and Petrology* **101**, 261–273.

Watson, E. B. (1979). Calcium content of forsterite coexisting with silicate liquid in the system Na_2O–CaO–MgO–Al_2O_3–SiO_2. *American Mineralogist* **64**, 824–829.

Wiser, N. M. & Wood, B. J. (1991). Experimental determination of activities in Fe–Mg olivine at 1400 K. *Contributions to Mineralogy and Petrology* **108**, 146–153.

Yang, H.-J., Kinzler, R. J. & Grove, T. L. (1996). Experiments and models of anhydrous, basaltic olivine–plagioclase–augite saturated melts from 0·001 to 10 kbar. *Contributions to Mineralogy and Petrology* **124**, 1–18.

Yoder, H. S. (1965). Diopside–anorthite–water at five and ten kilobars and its bearing on explosive volcanism. *Carnegie Institution of Washington Yearbook* **64**, 82–89.

Yoder, H. S. & Tilley, C. E. (1962). Origin of basalt magmas: an experimental study of natural and synthetic rock systems. *Journal of Petrology* **3**, 342–532.